# THE GLOBULAR CLUSTER POPULATION IN THE CORE OF THE COMA CLUSTER OF GALAXIES

by

René Kie Tanaja

Submitted in partial fulfillment of the

requirements for the degree of

Master of Science in Astronomy

Department of Astronomy and Physics

Saint Mary's University

Halifax, Nova Scotia

B3H 3C3



Submitted November, 1998

0-612-40359-9

## Contents

## Certificate of Examination

Saint Mary's University
Department of Astronomy and Physics

Dr. Michael J. West
Associate Professor
Department of Astronomy and Physics
Saint Mary's University
(Supervisor)

Dr. Malcolm Butler
Associate Professor
Department of Astronomy and Physics
Saint Mary's University

Dr. Gary A. Welch
Associate Professor
Department of Astronomy and Physics
Saint Mary's University

David G. Turner

Dr. David G. Turner
Professor
Department of Astronomy and Physics
Saint Mary's University

Dr. Sidney van den Bergh
Dominion Astrophysical Observatory
(External Reader)

The Globular Cluster Population in the Core
of the Coma Cluster of Galaxies

# Abstract

**René Tanaja**

November, 1998

In this study we attempt to discover, using data taken by Bernstein *et al.* (1995, Bea95), whether there exists a population of intracluster globular clusters (IGC) within the core of the Coma Cluster of Galaxies. Models are created in an effort to try to match the distribution of unresolved objects in the Bea95 catalogue within the globular cluster magnitude range at the distance of Coma, and tested using a two–dimensional, two–sample Kolmogorov–Smirnov test for compatibility. The best–fitting model was found to be composed of an 81% background component, an 18% NGC 4874 globular cluster component with a King–profile core radius of approximately 3.7′, and a 1% IGC component with a King–profile core radius of approximately 18′. Since the Bea95 background estimate from blank fields of similar galactic latitudes as the Coma field indicates that the background count in the Coma field accounts for only 74% of the unresolved objects in this range, it is possible that the remaining 7% of the objects found to belong to the background actually belongs to the similarly flat IGC component, raising its total count to 8% of the total number of objects. However, the $3\sigma$ uncertainty in the Bea95 background estimate leaves this possibility debatable. Tests of the effectiveness of the method and the similarity of the core radius values to those of X–ray distribution measurements seem to

confirm (within the $1\sigma$ uncertainty) that this model describes the true distribution correctly. However, model result and background count uncertainties are sufficient to prevent making a firm claim on the existence of IGCs. Better data is required to make this method truly viable in determining their presence.

# Acknowledgements

Behind every effort there is an army of people without whose support, nothing would be achieved. Above all, I must thank Mike West for all the advice and guidance, for allowing me to delve deeper into the beautiful depths of infinite space, and for the incredible patience while putting with me on my long stroll down parameter space. Great thanks to Sidney van den Bergh for taking the time from his exceedingly busy schedule to read my thesis. I also thank David Guenther for allowing me to explore some of the wonders back home in the Milky Way. More thanks to the other professors, in alphabetical order, Malcolm Butler, David Clarke, George Mitchell, David Turner, and Gary Welch. Thank you for the infinite insights, the inspirations, and help. Further thanks go to Dave Lane for answering all my stupid computer questions and hooking me up to all the computers I needed to use, and Shaun Mitchell for showing me all those neat things and for sharing all those interesting stories, along with all the physics insights. And, of course, loads of thanks to Elfrie Waters for taking me under her wing the day I got here, and to Karen for showing me around the Halifax area.

Many more thanks go to the occupants and former occupants of these hallowed halls of the grad rooms: Thanks to Kevin Douglas for putting up with my mess and all the inconsiderate things I may have done while we were roommates, as well as for sharing the gift of music and for showing me the ropes. To Juan Ramon Sanchez–Velar for the hot debates over lots of things as well as the help and insights. Thanks to Rachid Ouyed for an ungodly amount of help and letting me use Pandora once in a while. Also thanks to Andreea "Smiley" Font for the daily smile, great discussions, friendship, and shared experiences. And, of course, thanks to all of them for all the great times we had while hanging around town and traveling all over Nova Scotia. Also thanks to Beverly Miskolczi for sharing all those SciFi books, for listening to me rant and rave, as well as for the advice; to Dave Miskolczi for daring to freeze for those comet pictures; to Steve Shorlin for making me laugh my head off; to Gary Gidney for allowing me to borrow that amazing brain once in a while; and to Gong Yi for telling me all those great tales.

Still more thanks must go beyond these walls: To Tami Trenholm for all the camaraderie, the emotional support, and many other things I can't possibly list all of; to Andrew Horsford, Mel Johnson, Sue Fern, and all the other folks from SMUCAPS for the games and the friendship; and most certainly to Alex and Frank Leung, Jason Lee, Martin Kang, Lisa Snyder, Kakoli Mitra, my family, and everyone back home for believing in me, for all their support, and for all those moments in my life. Also a late, but infinitely significant, addition to the list, Jody Humphrey, for the extra inspiration in the last little while in the creation of this thesis. Their contributions go beyond mere words. Thank you all...

## List of Figures

## List of Tables

# 1. Introduction

## 1.1. Clusters of Galaxies

Clusters of galaxies (hereafter CoG) are among the largest structures in the universe. They contain from a few up to several thousand galaxies within a volume ranging upwards of several Mpc in diameter. Observations by X-ray satellites since the early 1970s (eg. Gursky *et al.* 1971, Forman *et al.* 1972, Kellogg *et al.* 1972, Jones & Forman 1978) revealed that the intergalactic space of CoGs is permeated by a component of hot gas which makes up from 10% to 20% of the total cluster mass (see reviews by Bahcall 1977, and Forman & Jones 1982; Sarazin, 1988). In addition, measurements from gravitational lensing by CoGs, such as Abell 370 (Lynds & Petrosian 1986 & 1989, Soucail *et al.* 1987) and Abell 2218 (e.g. Saraniti, *et al.* 1996), and of the virial dynamics of the member galaxies (Cowie, *et al.* 1987, Hughes 1989), indicate the presence of a dark matter component which makes up approximately 80% to 90% of the total mass. Furthermore, very recent deep images of CoGs have unveiled the existence of intracluster stars in the Virgo Cluster (Ferguson *et al.* 1998) and the Fornax Cluster (Theuns & Warren 1997), adding yet another constituent to the mélange of components. It is thus easy to see that CoGs are extremely complex objects to investigate and comprehend. To understand the history and evolution of CoGs, it is necessary to understand the characteristics and dynamics of the individual components, as well as their mutual interactions.

## 1.2. Globular Clusters

Globular clusters (hereafter GCs) are large, dense aggregates of stars, and are generally found in the haloes of almost all galaxies. They contain $\sim 10^5$ to $\sim 10^6$

gravitationally bound stars in a volume up to $\sim 50$ pc in radius, with core densities of up to approximately $10^4$ stars/pc$^3$ (Mihalas and Binney 1981). Isochrone fitting techniques and theoretical formation models imply that these objects are among the oldest in the universe, ranging in age from about $10 - 18 \times 10^9$ years in our galaxy. Although the highest of these values do exceed recent measurements of the age of the universe, resulting in an ages of approximately $12 - 14 \times 10^9$ years (Ferrarese *et al.* 1996, Freedman *et al.* 1998), attempts to reconcile the discrepancy are under way, and recent results from stellar modeling using the latest advances in the stellar physics theory are beginning to offer a glimmer of hope (Salaris *et al.* 1997).

The fact that GCs are some of the first stellar objects formed in the universe means that these objects are ideal for studying the history of their environments. Their generally low metallicities, for example, tell of the abundances of the elements within the first few billion years of the universe and during the epoch of formation of the galaxy, and their locations and dynamics provide clues to the formation process of the galaxy. The region closest to the centre of the galaxy is generally poor in cluster population, which supplies an indication to the orbits of halo objects as well as of the ability of the galactic centre in destroying passing objects (Tremaine, *et al.* 1975, Oort 1977,Capriotti & Hawley 1996).

### 1.3. Globular Clusters of Other Galaxies

With the advent of more advanced CCDs and improved telescopes, GCs have been detected in member galaxies of CoGs as far out as $\geq 70h^{-1}$ Mpc (e.g. Bernstein *et al.* 1995). The relative quantity of GCs which a galaxy possesses can be expressed by the *specific frequency* or $S_N$, formulation, defined as the total number of globular clusters per unit galaxy luminosity (normalized to $M_v = 15$), given by (Harris & van den Bergh 1981)

$$S_N = N_t \times 10^{0.4(M_v+15)}, \tag{1.1}$$

where

$N_t =$ the total number of globular clusters,

$M_v =$ the total absolute V magnitude of the parent galaxy.

The typical values of $S_N$ depends strongly on the galaxy type and environment (Harris 1991). Spiral galaxies have typical $S_N \leq 1$ (with $N \sim 10^3$ or less), while dwarf ellipticals have typical $S_N \sim 4-6$ (with the exception of the cluster - lacking M32 and the ultra–high $S_N$ Fornax Dwarf galaxy), and field ellipticals have $S_N \sim 2-4$. For ellipticals in rich clusters typical numbers are about $S_N \sim 5-8$, while for the giant ellipticals at the centres of the clusters (i.e. the D and cD–size galaxies) they can be as high as $S_N \sim 10-20$. These latter galaxies often have an entourage of many thousands of GCs which gives them their high $S_N$ values. For example, M87 possesses approximately 16000 GCs, giving it a $S_N \approx 14$ (Harris 1991, Harris *et al.* 1998, McLaughlin *et al.* 1994), while NGC 4874 in the Coma Cluster has approximately 21000 GCs (Harris 1987), with $S_N \approx 12$. However, not all cD galaxies have these enormous GC populations. The cD galaxy NGC 6166 (in Abell 2199), for example, has only $S_N \approx 4$ (Pritchet & Harris 1990). The reasons for these great variations are yet unknown, but they raise many questions on the generalizations of the role of the environment on the formation of GC systems of galaxies.

## 1.4. Intracluster Globular Clusters

The existence of globular clusters within CoGs not associated with the individual galaxies, but belonging to the cluster potential itself, was first suggested by White (1987) to explain the excessively large GC systems of several galaxies in CoGs, including M87 and NGC 4874 (Coma). This idea came from the suggestion of Merritt (1984) that the cD envelopes and the diffuse light in the Coma Cluster originate from stars tidally stripped from galaxies during the CoG collapse. If so, then GCs would be stripped along with the stars and create a population which belongs solely to the CoG potential. This population is then superposed onto the cD galaxy's own GC population to create an anomalously large specific frequency value.

This idea has been recently renewed by West *et al.* (1995). In their paper, they argued that the population of intracluster globular clusters (IGCs) is proportional to the cluster mass and that, assuming the X–ray gas is in hydrostatic equilibrium with the cluster potential well, the distribution of the X–ray gas directly traces the mass density of the cluster. This implies that by measuring the distribution of X–ray emission, one also measures the IGC density distribution. Since the central galaxy's location does not always correspond to the potential centre, the contribution from the IGC population to the galaxy's $S_N$ also depends on the distance of the galaxy from the centre of the potential well. They then showed that there exists a correlation between the excess number of GCs (assuming that a "normal" elliptical galaxy would have a $S_N \approx 4$) of a central galaxy and the local IGC density. A similar trend is also seen by Blakeslee *et al.* (1997) in a study of GCs in 19 Abell clusters.

The origin of the IGC population, however, is still unexplained. One explanation is that they are the debris remains of tidally stripped galaxies, but van den Bergh

(1984) pointed out that this process would increase the GC population in proportion to the halo stars, hence keeping the specific frequency of the parent galaxies constant. However, a study by Côté *et al.* (1998) of isolated galaxies indicate that the initial GC systems of galaxies may have been more spatially extended than the stars, hence early interactions would strip more GCs than stars off the interacting galaxies. However, Harris *et al.* (1998) argued that this would also produce some GCs with high velocities superimposed on the central galaxy, and their observations of M87 detected none. It is also possible that IGCs were created from the intracluster gas directly in the early epochs when density fluctuations may have been sufficiently high to allow the GC formation efficiency to become adequate to form the IGC population (eg. West 1993, Harris & Pudritz 1994). Fabian *et al.* (1984) suggested that they may have condensed from cooling flows, but Harris *et al.* (1995) found no correlation between $S_N$ and the present cooling flow rate. Finally, West *et al.* (1995) also suggested that they may have formed during the collisions of gas-rich subclusters.

The existence or nonexistence of IGCs is not a trivial matter. The presence or absence of these objects can be used to gauge the dynamic history of the cluster galactic components, as well as the degree of violence of interactions. It can also be used to investigate star formation history within the cluster and measure the strength of the cluster potential well in lieu of X-ray measurements.

### 1.5. Intracluster Globular Clusters in the Coma Cluster

The Coma Cluster of Galaxies is the richest of the nearby galaxy clusters, as well as one of the most studied. Its richness and closeness (approximately $70h^{-1}$

Mpc), along with the fact that it is close to a galactic pole (at $b = 88°$), establish it as a very convenient laboratory to study the characteristics and behaviour of galaxy clusters. The Coma Cluster also displays the presence of a substantial amount of dark matter and hot X–ray gas, and has been found to have substructure, which, in part, implies that it has not fully relaxed. It is hence a good test for dynamic models of galaxy clusters. (See, for example, Biviano 1997 and references therein.)

The presence of giant galaxies at the core, a deep potential well, and spiral galaxies which seem to have been stripped of their interstellar gas (van den Bergh 1976, Sullivan & Johnson 1978) implies that strong dynamic processes must have, and still do, occur within the cluster. This, along with the cluster's richness, mean that we can expect to see a substantial amount of tidal debris (e.g. Gregg & West 1998) within the intracluster medium, and hence, perhaps, a considerable population of GCs around the central region.

In 1991, Bea95 obtained a deep image of the core of the Coma Cluster of Galaxies. In the luminosity function that they obtained from the data they found an excess of objects at the low luminosity end of the distribution. They submitted that at these magnitude levels, globular clusters would be detected in addition to faint galaxies, and using the GC luminosity function available for M87, scaled to match the Coma data, they suggested that most of these excess objects at the low-luminosity end of the Coma Cluster luminosity function are probably detected GCs.

In this study we explore the possibility that most of these objects are indeed globular clusters and use this idea to test whether IGCs exist. The simplest way to achieve this is by attempting to recreate the distribution of objects found in the Bea95 catalogue by creating distribution models, with and without an IGC component, and compare each of these models to the real data. We model the unresolved object distribution observed by Bea95 using three–component models: one component for the GC population belonging to the cD galaxy (NGC 4874), one component belonging to the cluster potential (located apart from NGC 4874), and the rest belonging to an undetermined "background" population, which may include background galaxies and stars not accounted for in the background count determination. These models are then compared to the original data using the two–dimensional adaptation of the Kolmogorov–Smirnov test for goodness–of–fit. We thus hope to ascertain whether an IGC component can be found through association with the cluster potential component or an excess in the background counts compared to the Bea95 background counts, or both. If not, then perhaps we can determine some conditions for which IGC models can possibly hold true.

## 2. The Bernstein *et al.* Data

### 2.1. Observations

The original Coma Cluster field image was obtained by Bea95 on February 10, 1991 at the KPNO 4 m telescope, using a backside–illuminated 1024 × 1024 Tektronix CCD at prime focus, and an R filter. One pixel translates into 0.473″ in the sky on a side, giving a field of view of 8′ on the CCD. Twenty seven 300-second exposures were taken, each in a slightly different direction, as much as 1′ from the field centre, so that when co-added after debiasing and flat–fielding, cosmetic defects and cosmic rays could be removed. The images were then averaged, resulting in a high S/N image of approximately 7.5′ square (see Figures 2.1 and 2.2). The observations were nonphotometric, with up to 0.7 mag of obscuration by clouds, but later observations of the Coma field and a standard field on a photometric night on June 14, 1991 to determine the photometric zero–point of the deep Coma field revealed that the zero–point accuracy of the fields to be 0.05 mag or better, based on variance of standards and some repeat measurements.

The image is centred at $12^h57^m17.8^s$, $+28°09'18''$ (1950). The x-ray centroid is at the top, left of centre of the image (peak, at $12^h57^m26.2^s$, Ulmer *et al.* 1992), and the giant galaxies, NGC4874 and 4889, are 40″ of off the NW (upper right) corner and 280″ off the NE (upper left) corner, respectively.

In addition, five randomly–chosen, high galactic latitude fields were taken by Bea95 as control fields, with the constraints of low extinction and lack of bright stars or galaxies. They were not taken in the same observing run as the Coma field, but were taken on either the KPNO or CTIO 4-metre telescope, and were taken using also Tek1024 thinned CCDs. Image reduction techniques were the same as for the

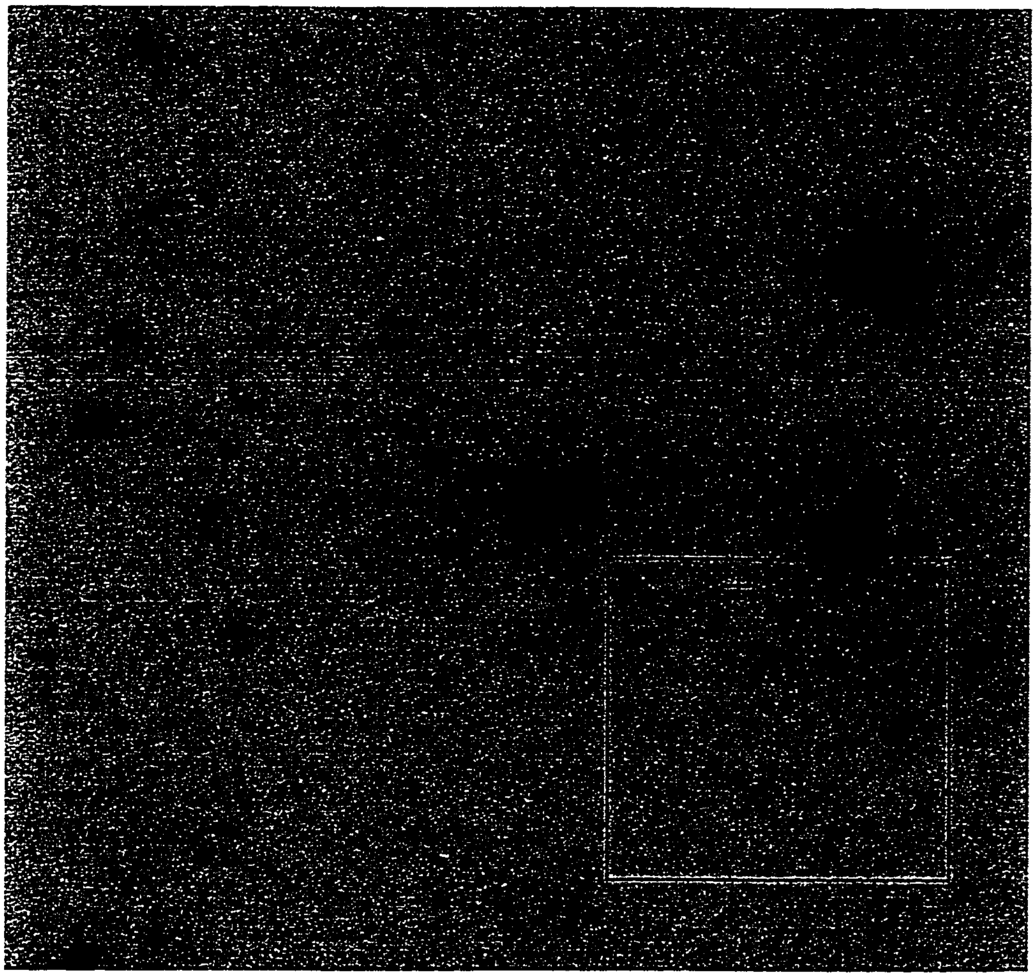

Fig. 2.1.— An image of the Coma Cluster central region obtained with the KPNO Burrell Schmidt telescope (Gregg & West 1998). The square indicates the Bea95 final image field, and the cross indicates the position of the X-ray peak. The giant galaxy at the centre is NGC 4889 and the giant galaxy to the right of centre is NGC 4874. The field of view is approximately 1° across. North is up, and East is to the left.

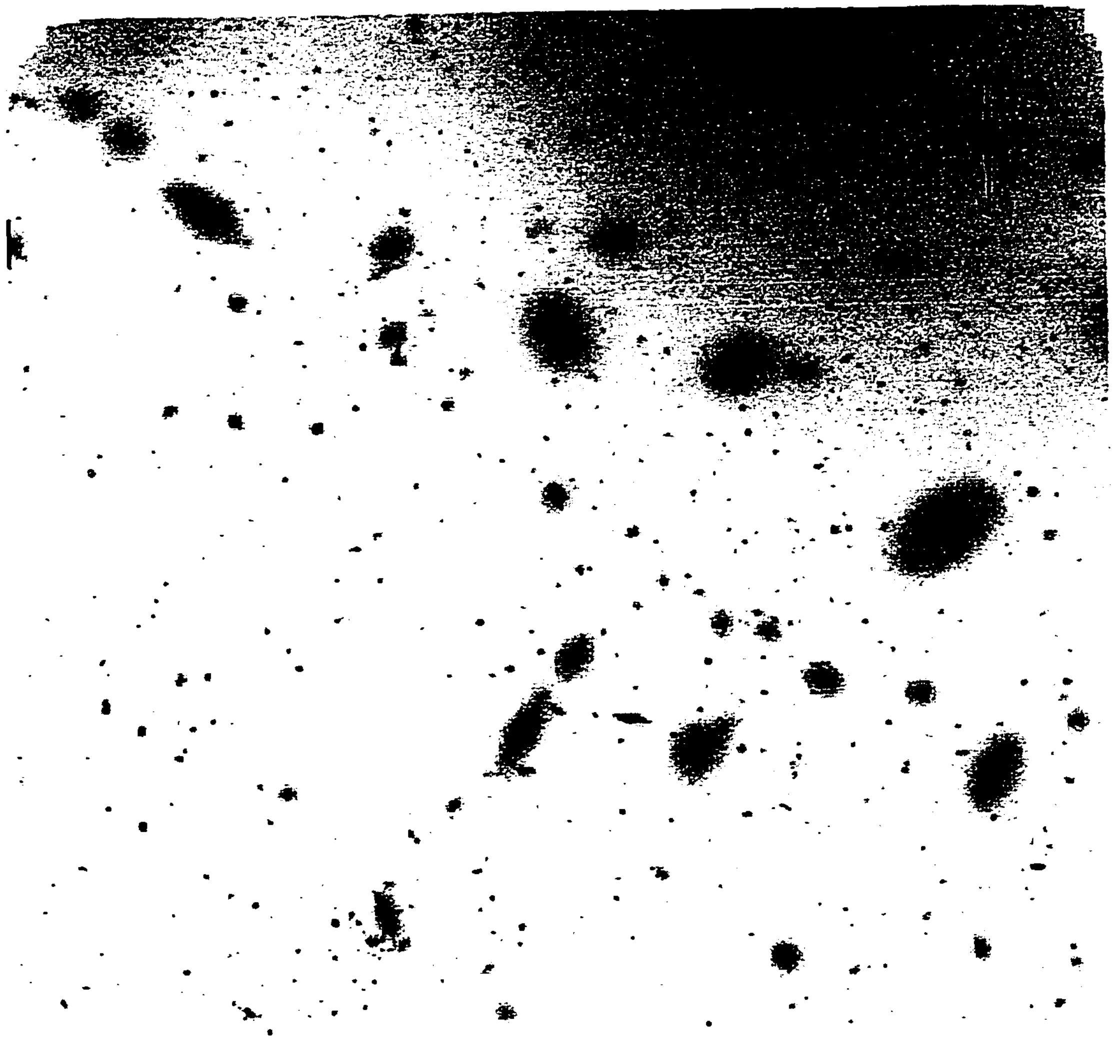

Fig. 2.2.— The full Bernstein *et al.* field image of the Coma Cluster core region. Field of view is approximately 7.5′ on a side, corresponding to approximately $150h^{-1}$ kpc. The giant elliptical, NGC 4874, is located just off the upper edge of the right portion of the image.

Coma image. These were then adjusted in detection characteristics (e.g. noise level and PSF) to match the Coma field.

Diffuse light in the Coma image (presumably from unresolved stars and galaxies) was then removed using subtractions of isophotal fits and FOCAS[1] "detect" program diffuse–light map, and median filtering. From comparisons of the KPNO and CTIO observations, it was concluded that the diffuse light is from the Coma cluster and not an artifact of atmospheric or telescope optics. FOCAS was also used to subtract the sky–level images from all of the observations, including the control fields.

## 2.2. The Catalog

The objects in the filtered image were catalogued using the FOCAS software package, which identifies pixels which exceed the local sky by more than $3\sigma$ (or 27.6 $R$ mag arcsec$^{-2}$ in these images), then links them to neighbouring pixels to form objects. The brightest objects were counted first, then they were masked or subtracted using elliptical isophote subtraction (Figure 2.3) to increase the contrast of the remaining image in order to detect the fainter objects. Faint objects centred within $5''$ of any masked region and edge were excluded from the list, to avoid photometry based on partially deleted apertures, as well as objects identified as bright foreground stars. At lower brightnesses, the stars are difficult to distinguish from the galaxies, and hence no differentiation was attempted. The magnitude measurements were adjusted for Galactic extinction, which amounted to 0.03 mag in the R–band for Coma.

[1]FOCAS, or Faint Object Classification and Analysis System, is a cluster of programs for creating and manipulating catalogs of objects from astronomical images.

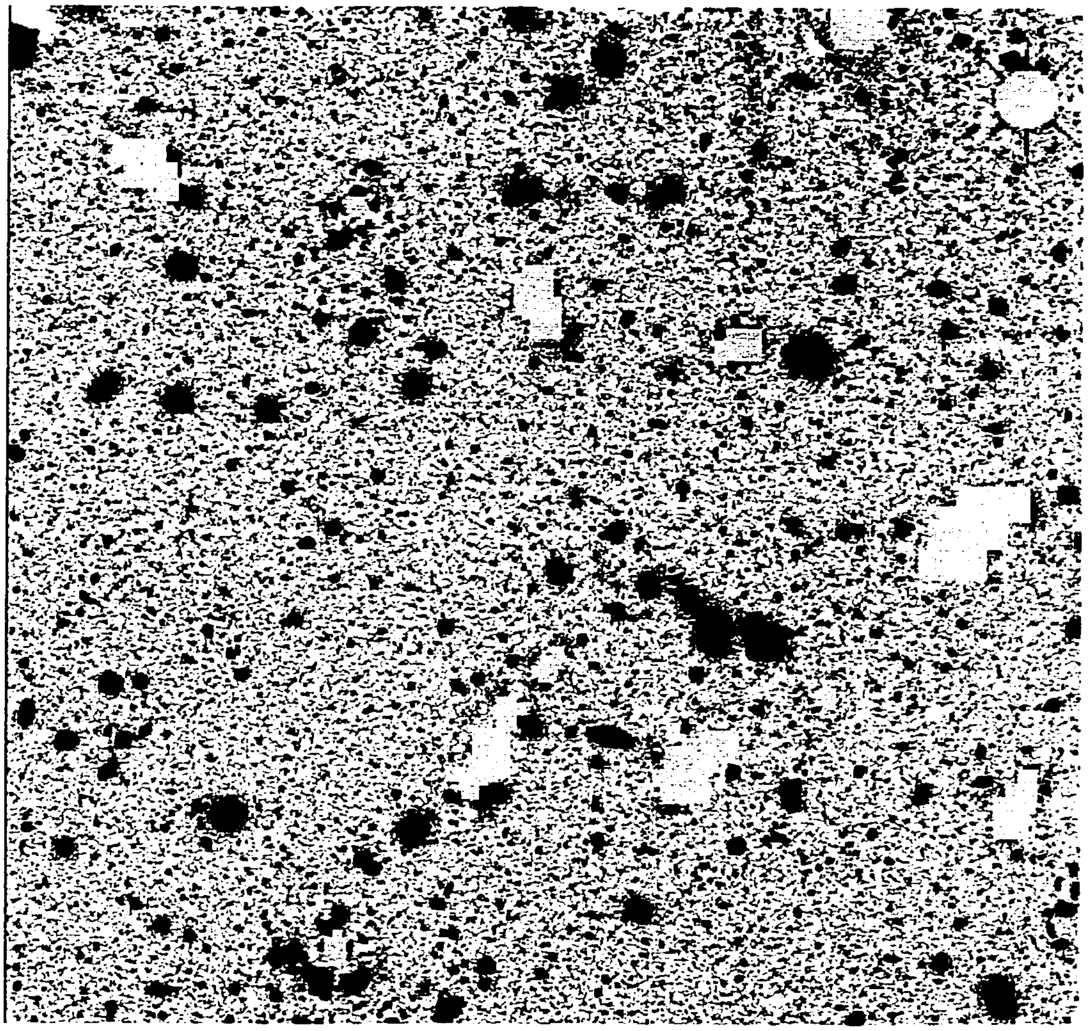

Fig. 2.3.— The Bernstein *et al.* final field with stars and the brightest objects masked or removed. The field of view is $7.5' \times 7.5'$, North is up, and East is to the left.

Completeness tests conducted by Bea95 revealed that the object detections in the Coma image are 50% complete for star–like objects at $R = 25.5$, and that the control fields match this to within 0.1 mag. The Coma field was found to be less complete at the $R = 24$ level because of the obscuration by remaining bright galaxies which had not been masked out. The counts were then compensated using detection probabilities for this region generated by Monte Carlo simulations.

The background counts in the Coma field are assumed to be the same as those of the control fields. The counts, however, can be affected by several factors:

1. The presence of intracluster dust in the Coma Cluster may reduce the background galaxy counts, which causes cluster galaxy counts to be underestimated.
2. The resulting luminosity function may be overestimated because the Coma field crosses the Great Wall, hence including some Great Wall members in the object counts.
3. The diffuse light component of the image may cause increase photon noise and affect detection efficiency, and the median filtering process may have removed the extremely diffuse cluster members and cause underestimation of counts.

## 2.3. Globular Cluster Candidates

Bea95 then used the object catalog to obtain a luminosity function (LF) for the Coma Cluster. The LF was parametrized using a power law $dN/dL \propto L^{\alpha}$, where $N$ the number of galaxies having a luminosity of $L$. The resulting LF exhibited two apparent regions: At $R < 23.5$ ($M_R < -11.4$, assuming $H_0 = 75$ km s$^{-1}$ Mpc$^{-1}$), the alpha parameter has a value of $\alpha \approx -1.3$, while at $R > 23$ ($M_R > -11.9$), this value becomes $\alpha \approx -2$. Since GC luminosity functions show that typically, $< M_v > \approx -7.4 \pm 0.2$ (Harris 1993), which translates into $< V > \approx 27.5$, and $< R > \approx 27.0$, assuming $V - R \approx 0.5$ (Harris 1996) and at a distance modulus of $m - M_v \approx 34$, the latter range is at the globular cluster detection region. The map of objects within this magnitude range is given in Figure 2.4. Using the assumption that the NGC 4874 GC population is a scale model of that of M87, and other arguments, Bea95 concluded that a great majority of the objects at this range are likely to be GCs. Hereafter, we will adopt as our study sample the objects detected in the Bea95 catalogue within this range of magnitudes, at $23.5 < R < 26.0$, where GCs are detected, and thus where IGCs may be found.

Bea95 clarified, though, that these detected objects cannot all be globular clusters. At the $R < 24$ level, detected dwarf galaxies are decreasing in size with decreasing luminosity, so at $R > 24$, their sizes are too small to be resolved at the Bea95 resolution limit. Furthermore, at fainter magnitudes their detection $S/N$ becomes too small to discriminate the objects by size, and Monte Carlo simulations show that at $R > 24.5$, they are impossible to distinguish from stellar objects (which have smaller PSFs). Finally, a higher resolution study by Thompson & Valdes (1987) of a nearby field within the Coma Cluster at $25.25 < B < 26.25$, which corresponds to about $24 < R < 25$, revealed a population of resolved dwarf galaxies and a population of unresolved objects, which they assumed to be GCs. Hence, a significant part of the population of unresolved objects is likely be made up of galaxies and very faint foreground stars.

## 2.4. Background Counts

In Table 2 in Bea95 (partially reproduced here as Table 1), in addition to the catalog counts of the Coma field, estimated background counts for individual magnitude ranges are also listed. These estimates were obtained from the mean object counts from the control fields at each magnitude range, corrected for areas and detection efficiencies to match the Coma field. The assumption is that the background count of the Coma field, $N_{bg}$ is drawn from the same population as the control fields, $N_i$. In the Coma count, this mean background population would account for approximately 74% of the total Coma population of unresolved objects from $R = 23.5$ to 26.0, within the magnitude range of the suspected IGC population. Within this range, therefore, we can expect that approximately this proportion of objects in the Coma catalogue belongs to unresolved background or foreground sources, and the rest belongs to the galaxy cluster itself.

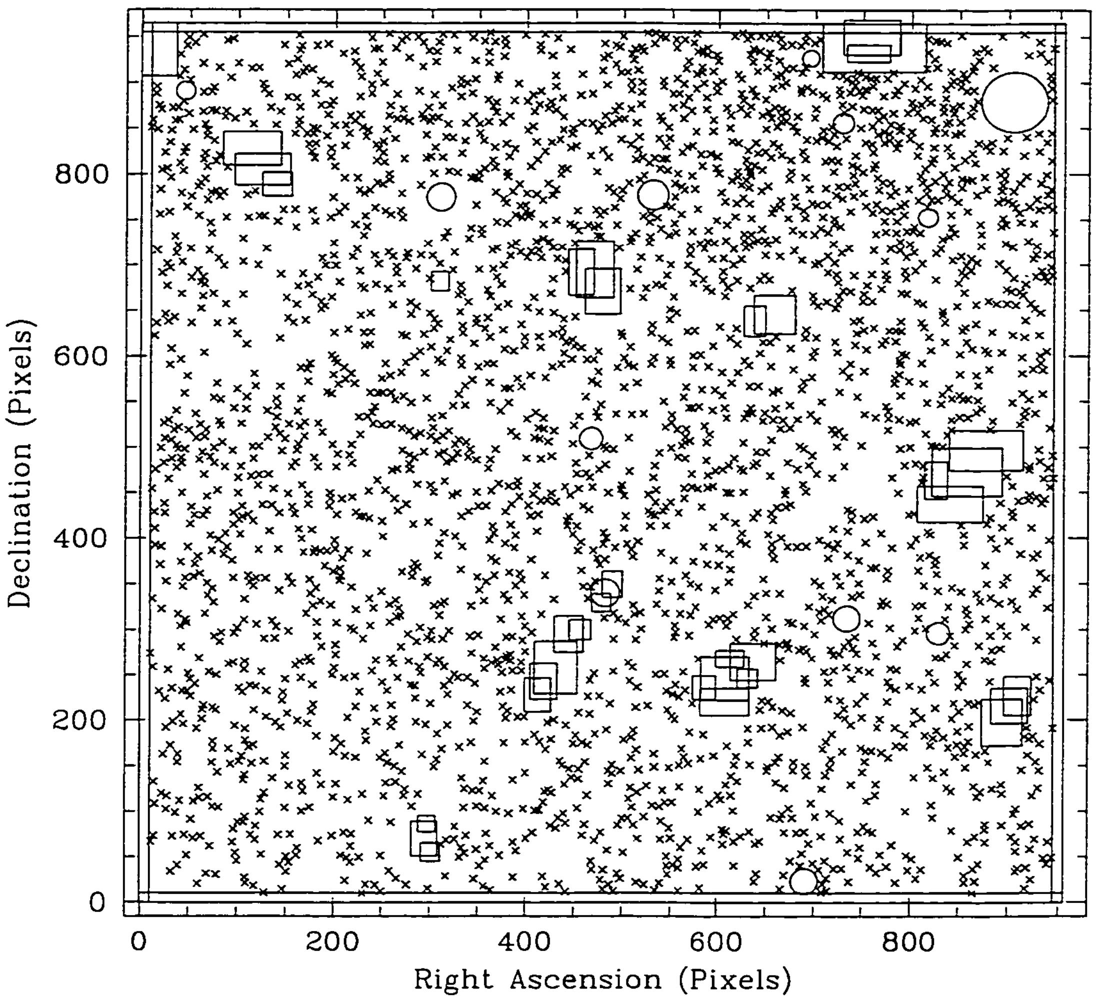


Fig. 2.4.— Map of the unresolved objects catalogued by Bernstein *et al.* from $R = 23.5$ to $R = 26.0$ and the masked regions.

| **R** | **N** | $\mathbf{N_{bkg}}$ | $\sigma_{\mathbf{bkg}}$ | **Percent Background** | $\sigma_{\mathbf{pb}}$ |
|---|---|---|---|---|---|
| 1 | 2 | 3 | 4 | 5 | 6 |
| 23.5–24.0 | 395 | 311.33 | 26.61 | 78.8 | 6.7 |
| 24.0–24.5 | 532 | 381.58 | 27.52 | 71.7 | 5.3 |
| 24.5–25.0 | 658 | 476.78 | 32.34 | 72.5 | 6.3 |
| 25.0–25.5 | 739 | 522.40 | 71.72 | 70.7 | 9.7 |
| 25.5–26.0 | 574 | 446.63 | 57.63 | 77.8 | 10.0 |
| **Net** | 2898 | 2138.72 | 104.77 | 73.8 | 3.6 |

Table 1: Object and background counts of Bernstein *et al.* for bins of 0.5 magnitude in the range of the unresolved objects. Column 4 is the uncertainty in the background count, column 5 is the percentage of the background count relative to the object count, and column 6 is the uncertainty in the percentage of the background count relative to the object count.

## 3. The Two – Dimensional Kolmogorov – Smirnov Test

As previously mentioned in Chapter 1, we attempt to find a population of IGCs within the Bea95 data by modeling the distribution of unresolved objects in the Bea95 catalogue using multi–component simulations. We compare the created set of models with the real data and then choose the best–fitting model as our best description of the object distribution. In this way, we hope to discover a population which is unaccounted for by the NGC 4874 population or the background galaxy counts.

To measure the similarity between our models and the Bea95 distribution, we require an efficient and effective goodness–of–fit test, especially because of the number of data points considered and the number of models we need to create in order to focus in on the correct parameters. In the one–dimensional case, perhaps the simplest, most efficient of these tests is the Kolmogorov–Smirnov test (hereafter KS test), which determines poorness–of–fit by measuring the greatest absolute difference between two cumulative distributions, and expresses it as the KS "$D$" statistic (see Figure 3.1) (or, more appropriately, the quantity, $Z \equiv D\sqrt{n}$, where $n$ is the size of the distribution). To find the model which simulates the real distribution best, one merely needs to find the model which results in the lowest value of $D$.

The advantages of the KS test are well–known (see, for example, Peacock 1983). It is a highly sensitive test of likeness, and its simplicity avoids the need for extensive calculations, making it also very efficient. It is also a very comprehensive test in the way that each individual data point is considered so that it produces a statistically complete picture of the comparison. Furthermore, the KS test is independent of ordering direction, and since it is a non-parametric test, it does not

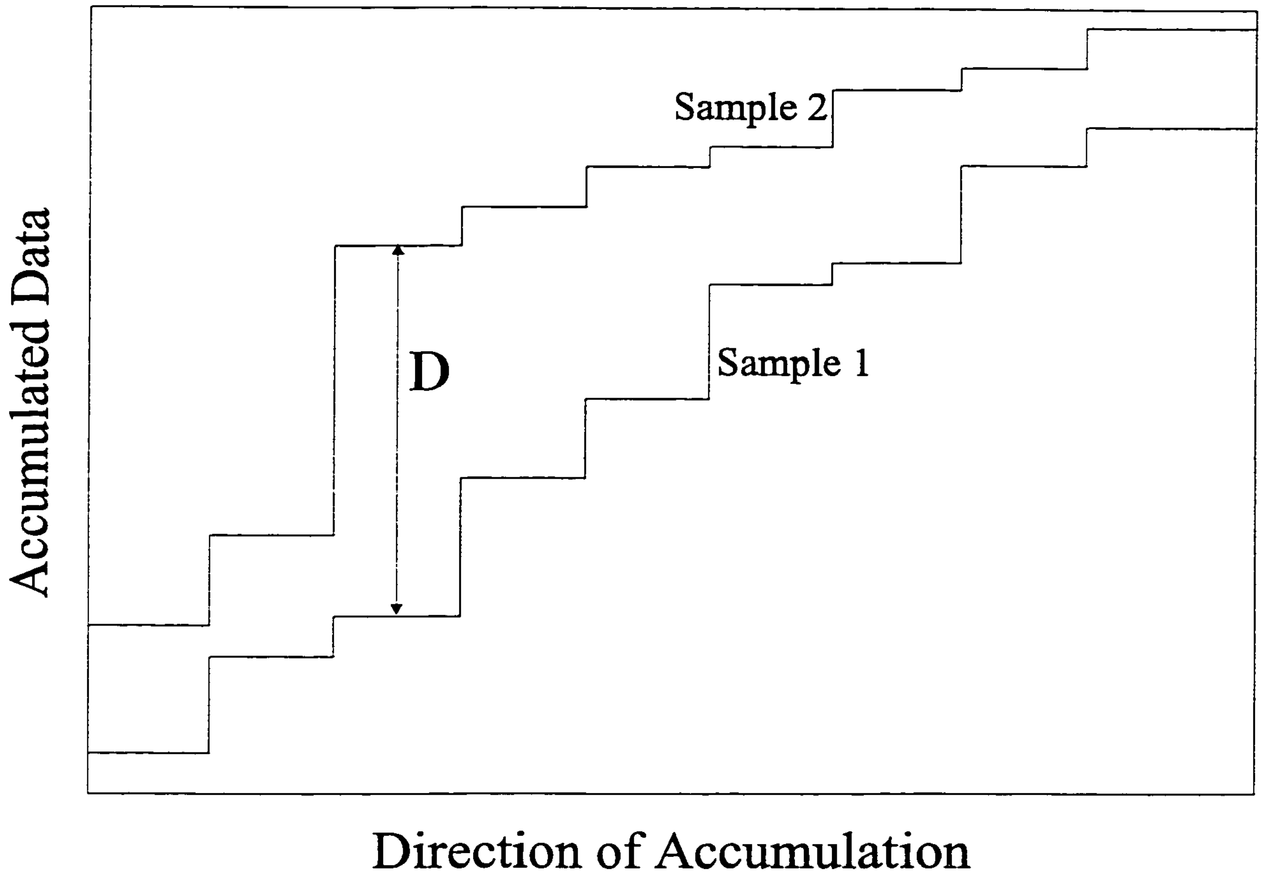


Fig. 3.1.— The Kolmogorov–Smirnov test "$D$" statistic (in one dimension). It is defined as the greatest absolute difference between two cumulative distributions.

require any assumption about the underlying parent distribution. However, these are all rigorously true only for the one–dimensional case.

For two–dimensional (and higher) distributions, obtaining the $D$ statistic using the KS test is no longer simple. The extension of the cumulative probability distribution to the two–dimensional case can be defined in a very straightforward way as the probability that a data point would reside at $x < X$, $y < Y$, and so forth, where X and Y is taken as the coordinates of one of the data points, and the process is repeated for all data points. This preserves the data–point–comprehensiveness of the one–dimensional test. The problem lies mainly in the directions which the data points are ordered in the different dimensions. In one dimension, the two directions available for counting are not independent of each other, hence one direction is as good as the other. However, in the two-dimensional case, since there are two dimensions in which the data points can be accumulated and each dimension has two directions in which the cumulation can be done, one can choose any one of four possible combinations of directions from which to obtain the $D$–statistic, only two of which are independent of each other. Which is the one to use is far from clear. In general, for $N$ dimensions, there are $2^N - 1$ independent ways of counting, resulting from all the possible combinations of counting directions, making the determination of $D$ very complicated.

Peacock (1983) suggested that the simplest way to solve this quandary in the two–dimensional case is to define the $D$–statistic to be the maximum absolute difference between the two cumulative distributions when all independent combinations of ordering are considered. Since each of the four quadrants created by considering each coordinate pair is an equally valid region for cumulating data points, all four quadrants must also be considered separately. However, as pointed out by Fasano & Franceschini (1987, hereafter, FF87), because each dimension has a separate set of coordinate values, for absolute completeness, all possible coordinate pairs must be considered, resulting in $4n^2$ calculations when all quadrants from all possible pairs are considered. For large values of $n$, the calculation of $D$ would require copious computing time.

In their paper, FF87 showed that instead of using the $n^2$ points for accumulating the data points for calculation of $D$, Peacock's method can be adapted to use only the $n$ data points of the distribution. This has the practical advantage of allowing the testing of distributions with considerably larger populations without significant cost in computing time while retaining the completeness of using all data points as well as most of the simplicity of the KS test. They conducted Monte Carlo tests to investigate the validity of this idea and confirmed that this method is just as legitimate as the full version of Peacock.

Another major concern of both Peacock and FF87 is that by taking the KS test to higher dimensions (than one) in this way, the test is no longer necessarily distribution–independent, that is, the outcome of the test may be different for different distributions even if the intrinsic goodness–of–fit is essentially the same. Monte Carlo tests conducted by Peacock for regular to highly "pathological" distribution patterns on the full version, however, indicated that, unless the distribution is strongly correlated, this test is sufficiently distribution–independent for most applications, and the resulting significance level calculations will deviate from the true value by $\sim 50\%$ at most. Similar tests by FF87 on the "improved" version indicated that there is a weak, but significant, dependence of the statistics on the correlation coefficient of the distribution, so that once the correlation coefficient is accounted for (via a polynomial fit relating the test critical values of $Z$ to $n$, the correlation coefficient, and the significance level), the resulting statistics can be declared essentially distribution–independent within the $3\sigma$ level. This also means that the problem Peacock encountered with strongly correlated distributions is averted, since its cause has been identified and reckoned with.

For a two–sample case, both Peacock (1983) and FF87 found that their versions of the two–dimensional KS test (hereafter 2DKS) are both as valid as for a one–sample case, with a few adaptations. Since there are two separate sets of data points to consider, two $D$–values will be generated, both of which must be accounted for. FF87 found that, using Monte Carlo simulations to confirm their hypothesis, it is appropriate that the $D$–value reported simply be the average of the two $D$ values, or $\bar{D}$. In calculating $Z$, the equation is adapted so that:

$$Z = \bar{D}\sqrt{\frac{n_1 n_2}{n_1 + n_2}}, \tag{3.1}$$

where $n_1$ and $n_2$ are, the sizes of the two samples. They found that, using this formula, the probability distribution of $Z$ is indistinguishable from that of the one–sample case. This means that significance levels can be calculated simply using the critical $Z$ values from the one–sample case, with the assumption that the two correlation coefficients are not significantly different; thus the degree of goodness–of–fit can be easily obtained using the more easily determined values.

The significance level of the resulting value of $Z$ for a large value of $n$ ($\geq 80$) can be expressed as (Kendall & Stuart 1979):

$$P(Z > Z_{observed}) = 2\sum_{k=1}^{\infty}(-1)^{k-1}e^{-2k^2 Z}. \tag{3.2}$$

With the normalization using the correlation coefficient, we can replace $Z$ on the left side (as represented by Equation 3.1) with the formula (Press *et al.* 1992, Section 14.7):

$$Z' = \frac{\sqrt{n}D}{1 + \sqrt{1 - (r_1^2 r_2^2/2)(0.25 - 0.75/\sqrt{n})}}, \tag{3.3}$$

where:

$$n = \frac{n_1 n_2}{n_1 + n_2}, \tag{3.4}$$

and $r_1$ and $r_2$ are the correlation coefficients of the two distributions. This formula, however, is only an approximation and is accurate enough for $P \leq 0.20$, but may not be accurate when $P > 0.20$. Yet, the implication is correct that the two distributions are not significantly different and that one model is a better comparison than another. Thus, despite the limitation of this approximation, calculating $P$ this way does indicate that the best–fitting model is significantly similar and is the best fit of all the models tested. It also gives a sufficiently accurate indication of the significance limit of the models at the $P = 0.05$ level. This is important, since models cannot be completely rejected as long as $P > 0.05$.

In our experiment, however, it was found that the value of the calculated significance level has a significant scatter from one random realization of a model to another. To account for this effect, the same model is run several times, each time with a different random number generator seed value. The final value of $\bar{D}$ and $Z'$ to be used is taken as the mean of the results of the individual runs of each model[2]. This appears to be appropriate, since the relationship between $\bar{D}$ and $Z'$ was found to be very linear (see Figure 3.2). The significance level of the match between each model and the Bea95 distribution is thus calculated from this value of $Z'$.

---

[2]Since the calculation of $Z'$ requires a value of $D$, for each of the multiple runs of each model, the $Z'$–value is calculated using the run's own generated $D$–value.

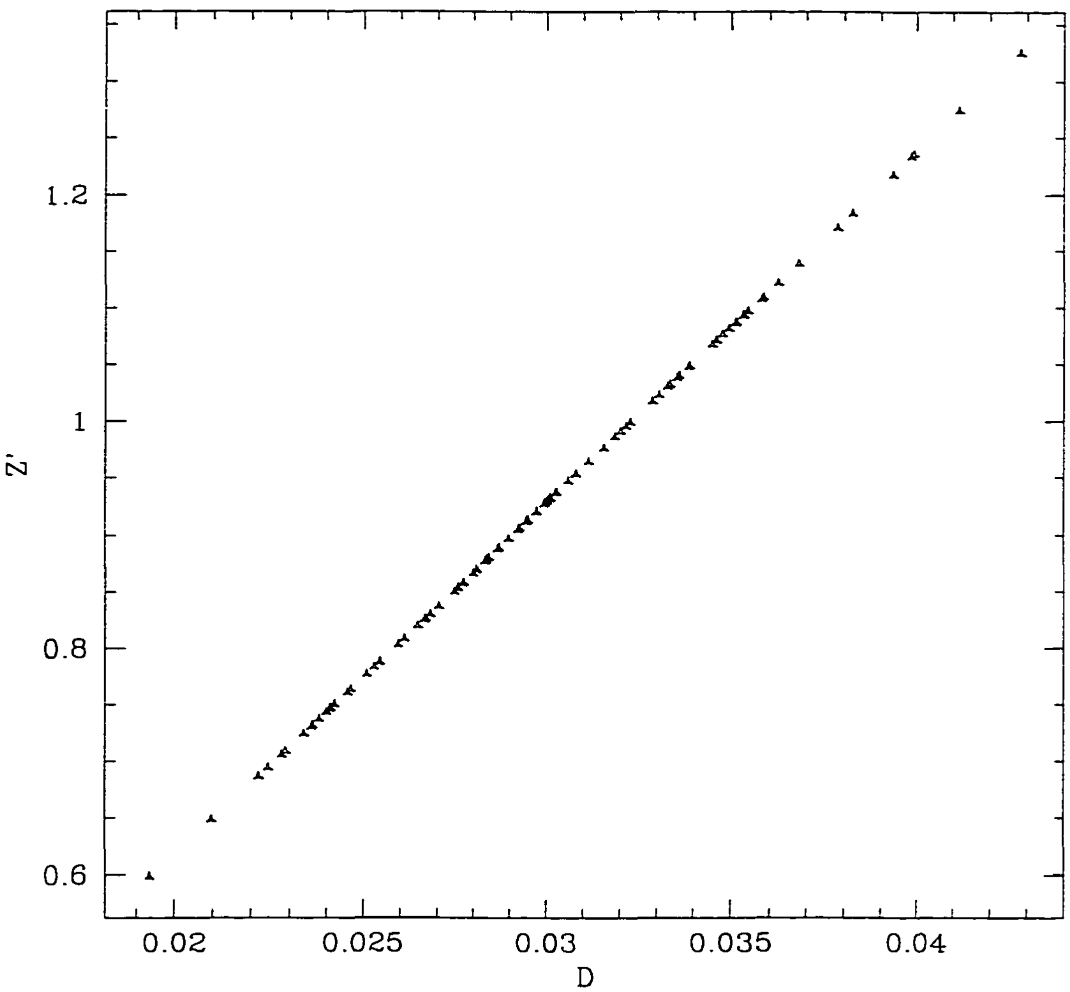


Fig. 3.2.— An example of the linearity of $Z'$ vs. D for a model. There are 100 data points plotted, and correlation coefficient is better than 0.99.

# 4. Models

The models created here are made in order to attempt to recreate the distribution of unresolved objects found by Bea95 within the range of $R = 23.5$ to $R = 26.0$. As previously mentioned, these models consist of three components, one belonging to NGC 4874, one belonging to the centre of the cluster potential (assumed associated with the X-ray distribution centre), and the last belonging to a flat background population which represents background galaxies and foreground stars. Thus, we begin with the *a priori* assumption that there exists an IGC population belonging solely to the cluster potential, but we also allow for models which do not have an IGC component. We then search for the best-fitting model or set of models and examine the results to find out whether such a population exists or whether the conditions for which such a population exists can be restricted.

## 4.1. The Simulator Program

The purpose of the computer code is to create model two-dimensional distributions to simulate the distribution of objects obtained from the Bea95 catalogue, and then use the two-dimensional, two-sample KS test to assess the similarity between each model and the observational data. It is designed to create a specified number of models in a batch run. As described in Chapter 3, each model is run for a specified multiple number of times (hereafter referred to as "sub-runs"), each time using a different random number generator seed value, and the resulting $\bar{D}$ and $Z'$ values (the latter then used to calculate the significance level) are taken to be the average of those of the individual sub-runs.

Several additional parameters are also to be specified to run the models. They include: the size of the field, the number of components, the type of distribution for each component (see below), the central position of each component, the relevant parameters of each component (e.g. core radius), and the percentage of the total population which belongs in each component. There is also an option to include a subroutine which deletes sections of the model distribution to match the real data. which is used in the real model runs, but is not used for the test runs (see the next section).

Once the number of GCs belonging to each component has been calculated (from the total number of objects and the specified percentage belonging to each component), the component distribution is created in turn by calling the appropriate subroutine for creating the distribution type. The currently available distribution types are: (i) random background and (ii) King Profile (King 1966):

$$\Sigma(r) = \frac{\Sigma_0}{1 + (\frac{r}{r_c})^2}, \tag{4.1}$$

where $\Sigma$ is the surface density at radius, $r$, $\Sigma_0$ is the central surface density, and $r_c$ is the core radius, the radius at which the surface density falls to half the central value. The background profile is a uniform random distribution within the image size limits, while the King profile is defined by randomly generated radial positions, based on their respective distribution density profiles, and randomly generated angular positions. If a generated pair of coordinates falls within one of the deleted sections of the Bea95 image (which accounts for 9.3% of the image area), it is rejected and another one generated. The combined distribution is then tested with the KS tester for goodness-of-fit to the Bea95 distribution. Each of the distribution-creating subroutines employs the random number generator in Press *et al.* (1992, p. 267) called "ran3".

The procedure in the previous paragraph is repeated for each sub–run, and once the entire set of model sub-runs is complete for a given set of input parameters, the average value of $\bar{D}$ and $Z'$ are calculated. From the generated $Z'$–value, the significance level of the model's goodness–of–fit is then calculated. All three of these values are then recorded, along with the resulting statistics from each sub run and the input parameters of the model. The minimum value of averaged $\bar{D}$ among the generated models in the batch run is then determined and rerecorded at the end of the result file along with its corresponding input parameters and related statistics.

The two–dimensional, two–sample KS tester used in this program was obtained from Press *et al.* (1992, p. 614), which employs the FF87 version of the 2DKS test. It also employs several support subroutines from various other sections of the book.

## 4.2. Program Tests

In order to gauge the effectiveness of the program and of our adopted methodology, we conducted several test runs using the program. Each successive test uses a more complicated distribution to be modeled (hereafter referred to as the "parent model") than the last, and is run using the same basic conditions as the Coma runs (e.g. the centres of the distributions are fixed and defined) (see the next section). Each parent model is generated using a program similar to the model generator above, and the distribution is confined to a box of $1000^2$ pixels in area, although the centres of the components are not necessarily within the box. Zeroing in on the best–matching model is done in the same way as for the Coma runs (see next section).

The first test parent model was simply composed of two distributions, both with King profiles. One component possessed 68% of the total population, with a core radius of 150 pixels, and the other was composed of the remaining population with a core radius of 800 pixels. The second test parent model was composed of only one distribution of the King type, with a core radius of 400 pixels. The models for this test distribution, however, were created as if there were two distributions, the second being supposedly centred to the upper left corner, outside the field. This was done in order to investigate the simulator's response to a nonexistent population distribution. The third was made up of three components, as was to be modeled for the Coma data, with two King components, making up 32% and 36% of the total population, with core radii of 200 and 500 pixels, respectively, and one background component constituting the remainder. The fourth test model was similar to the third, but with the background dominating at 80%. Its King components have compositions of 15% and 5%, and core radii of 300 and 500 pixels, respectively. All the total population sizes were similar to that of the Bea95 data. The results are given in Table 2. The test distributions and their respective best matching model distributions are displayed in Figures 4.1 to 4.10.

The test runs show that the program is quite capable of finding the correct parameters for a given distribution of objects. The component percentage compositions were found to differ from the test parameters by only a few percentage points for each of the cases. There is, however, a noticable trend with respect to the core radii parameters of worsening agreement with larger values of the test core radii (with the possible exception of the third test). It appears that the larger the test core radius value, the more the program underestimates this parameter, from little or no disagreement for core radii of $\approx 200$ up to almost 150 pixels at core radii of $\approx 800$.

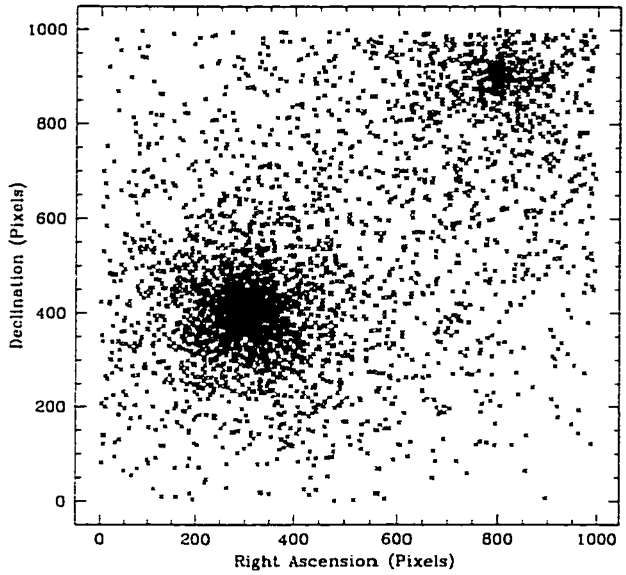


Fig. 4.1.— Distribution for the first test of the program. There are two components, both with King-type profiles.

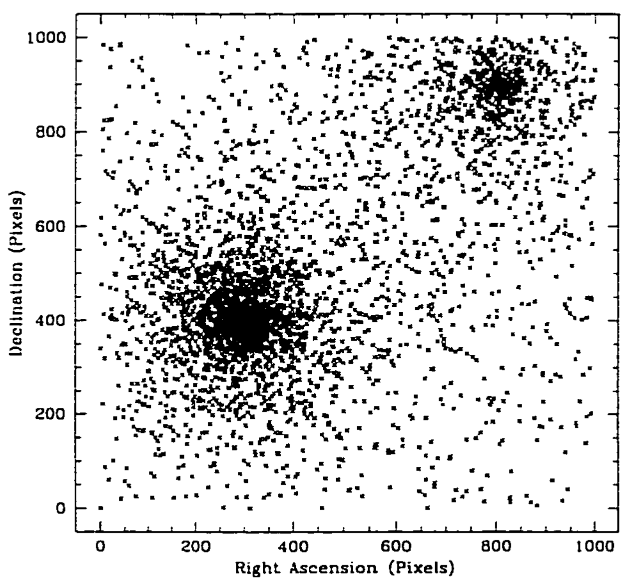


Fig. 4.2.— The best-fitting model, according to the 2DKS test, for the first test distribution.

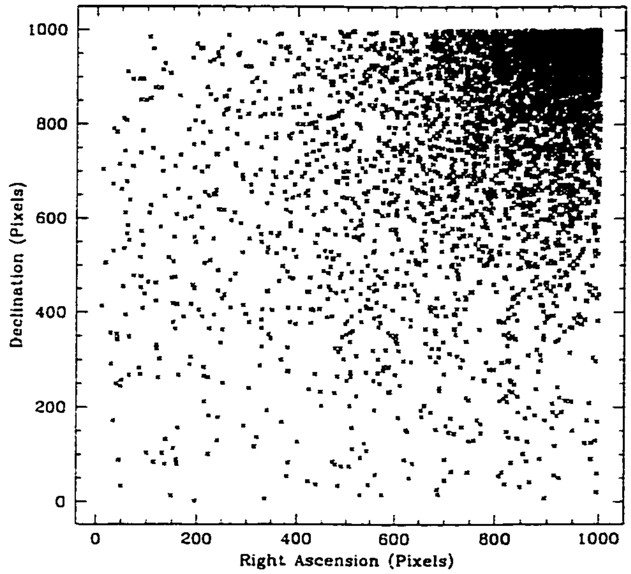


Fig. 4.3.— Distribution for the second test of the program. There is only one component, with a King profile and centroid at the upper right corner of the simulated region.

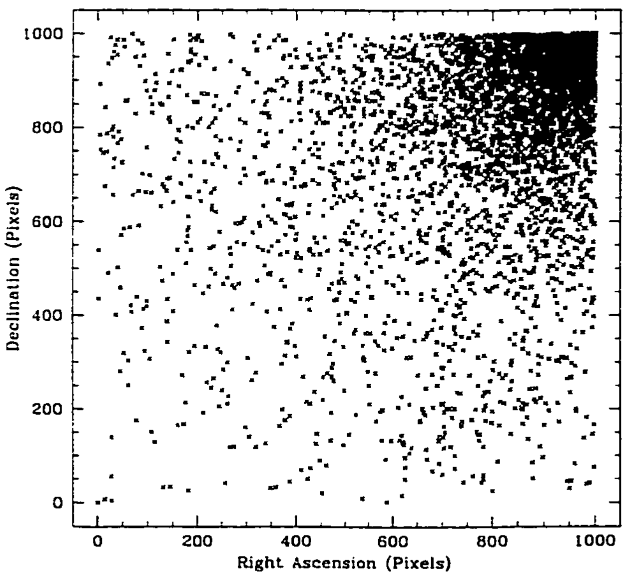


Fig. 4.4.— The best-fitting model, according to the 2DKS test, for the second test distribution.

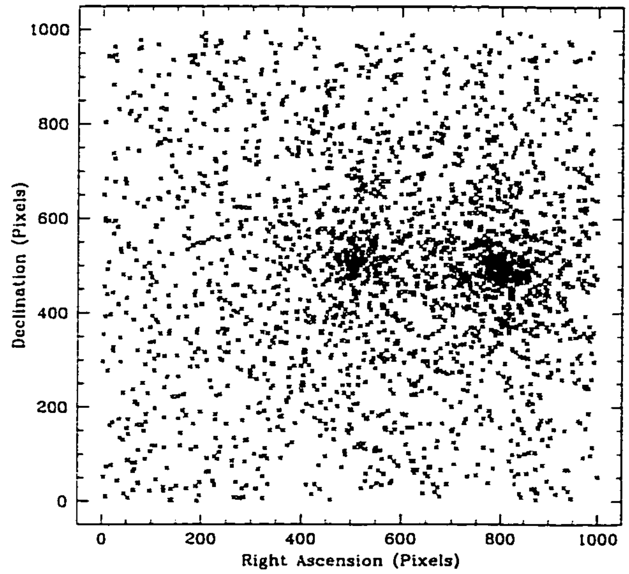


Fig. 4.5.— Distribution for the third test of the program. There are three components, two with King profiles, plus a random background.

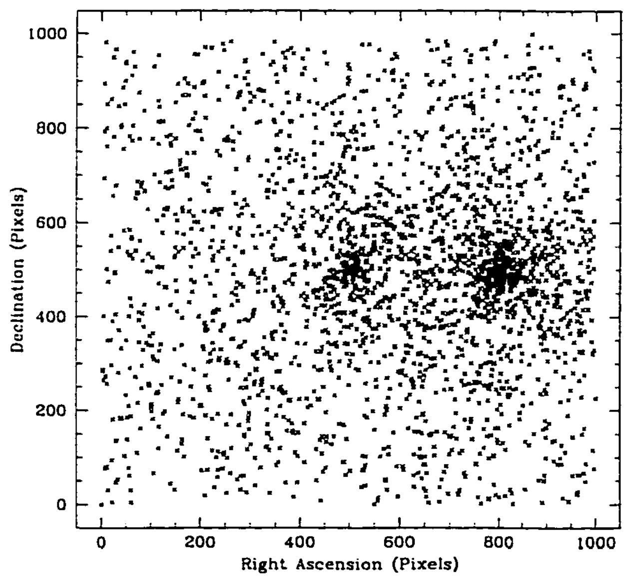


Fig. 4.6.— The best-fitting model, according to the 2DKS test, for the third test distribution.

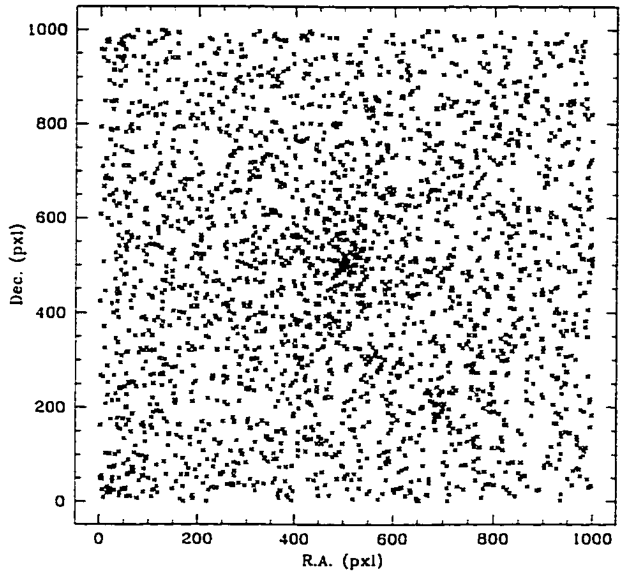


Fig. 4.7.— Distribution for the fourth test of the program. There are three components, two with King profiles, plus a random background.

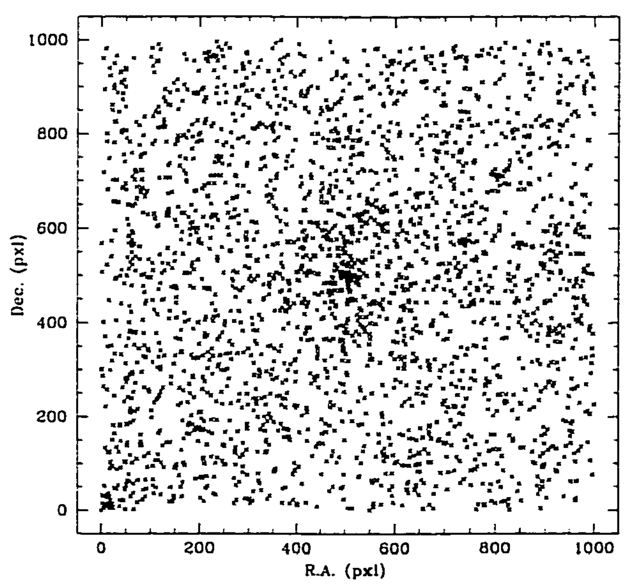


Fig. 4.8.— The best–fitting model, according to the 2DKS test, for the fourth test distribution.

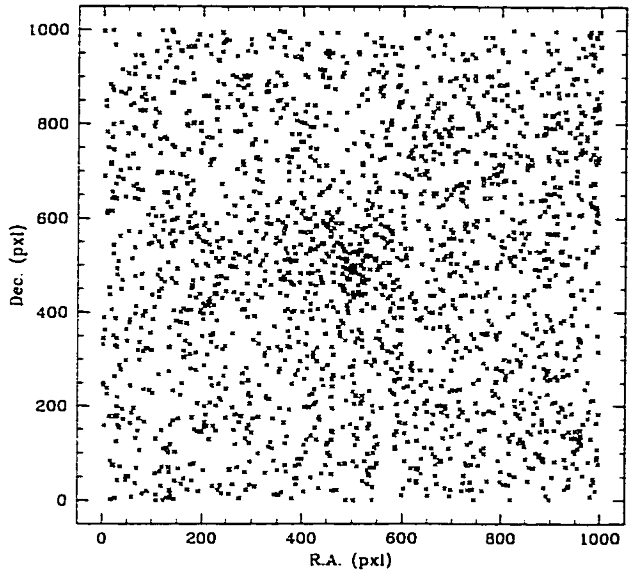


Fig. 4.9.— Distribution for the fifth test of the program. There are three components, two with King profiles, plus a random background.

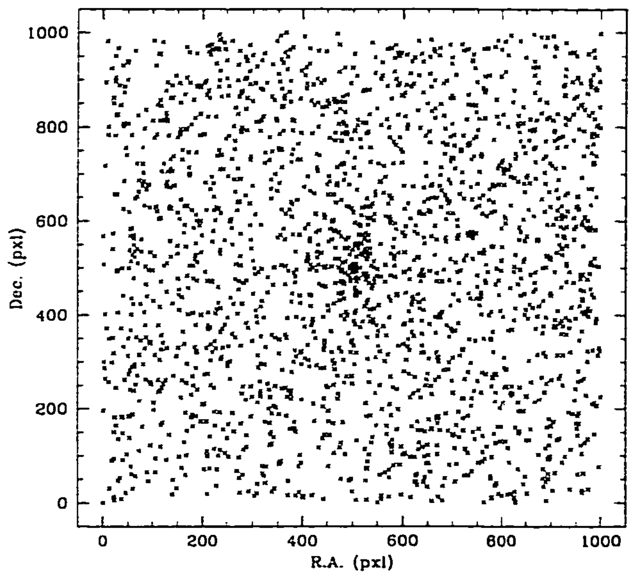


Fig. 4.10.— The best-fitting model, according to the 2DKS test, for the fifth test distribution.

| | Comp. | Comp. | Test Simulation | | Best Model | | | |
|---|---|---|---|---|---|---|---|---|
| | No. | type | % | $R_c$ | % | $R_C$ | $\bar{D}$ | Sig. Level |
| **Test 1** | **1** | King | 68 | 150 | 69 | 160 | 0.02471 | 0.311 |
| | **2** | King | 32 | 800 | 31 | 660 | | |
| **Test 2** | **1** | King | 100 | 400 | 99 | 310 | 0.02421 | 0.0311 |
| | **2** | King | 0 | – | 1 | $> 1200$ | | |
| **Test 3** | **1** | King | 32 | 200 | 33 | 200 | 0.02989 | 0.450 |
| | **2** | King | 36 | 500 | 34 | 550 | | |
| | **3** | Back. | 32 | – | 33 | – | | |
| **Test 4** | **1** | King | 15 | 300 | 20 | 470 | 0.03121 | 0.399 |
| | **2** | King | 5 | 500 | 5 | 590 | | |
| | **3** | Back. | 80 | – | 75 | – | | |
| **Test 5** | **1** | King | 18 | 400 | 13 | 230 | 0.03694 | 0.314 |
| | **2** | King | 8 | 1200 | 6 | 1280 | | |
| | **3** | Back. | 74 | – | 81 | – | | |

Table 2: "Parent model" parameters and the results of the tests. $R_c$ is the core radius of the King profile. The search step size in percentage is 1%, and the step size in core radius is 10 pixels, except for component 2 of the second and third tests, where the step sizes were 100 and 50 pixels, respectively, and the second King–profile component of the fifth test, with a core radius step size of 50 pixels.

This can be explained by the fact that as test core radius increases, the distribution of points belonging to the component becomes flatter. This in turn increases the ambiguity concerning which component the data points belong to, especially where the individual distributions overlap. In the first test, this translates into part of the second component's distribution being assigned to the first component, giving the latter a slightly larger percentage and core radius and slightly truncating the second component. In the second test run, it assigns the outermost data points to the "fictional", much flatter, second component, resulting in the truncation of the first component. In the third test, it causes more data points to be given to one of the King components and the background component at the cost of the second King component, also increasing the latter's percentage composition. In the fourth test the background component loses some of its population to the outer region of one of the King–profile components. In the fifth test, more is assigned to the background component, mostly at the cost of the larger King–profile population and partly at the cost of the smaller King–profile population. In this case, it is also worth noting that the core radius value of the smaller King–component matches that of the test value very well. With the fourth and fifth tests, it is shown that with a large background population and a large King–profile core radius, it is very difficult to obtain the correct parameters.

Nevertheless, these tests demonstrate that this program is very adequate for the purposes of our experiment.

## 4.3. Application to the Coma Cluster Data

### *4.3.1. Component Coordinates*

To be able to accurately model the distribution of the unresolved objects in the Bea95 image, it is necessary that the positions of the component centres be determined accurately. However, it was found that the coordinates specified for the centre of the image given in Bea95 paper are insufficiently accurate to be useful (since their research required only that the image is at the core of the Coma Cluster, they did not need to accurately specify the centre of the image). Compared to the listed positions of other bright galaxies in the image, the determined positions of the centres of NGC 4874 and the X–ray centroid were found to deviate from the correct location by as much as 200 pixels in right ascension, and as much as 50 pixels in declination.

In order to correct for this discrepancy, four bright galaxies within the image with well-determined positions were used; the positions of NGC 4874 and the X-ray gas component were then determined relative to the positions of these galaxies in the image. The galaxies used were: NGC 4875, NGC 4876, IC 3973, and IC 3976[3]. In the image, the position of the galaxies were determined by measuring the geometric centre of the images from the major and minor axes. The relative positions of the component centres were then averaged from the two most consistent results, and

[3]All coordinates, epoch 1950, were obtained from NED. Where two recent and accurate coordinates were given, the average of the two were taken. The NASA/IPAC Extragalactic Database (NED) is operated by the Jet Propulsion Laboratory, California Institute of Technology, under contract with the National Aeronautics and Space Administration.

| **Object** | R.A. | Dec. |
|---|---|---|
| NGC 4875 | $12^h57^m12.90^s$ | $+28°10'35''$ |
| NGC 4876 | $12^h57^m19.60^s$ | $+28°10'55''$ |
| IC 3973 | $12^h57^m05.90^s$ | $+28°09'12''$ |
| IC 3976 | $12^h57^m04.45^s$ | $+28°07'09''$ |
| NGC 4874 | $12^h57^m10.89^s$ | $+28°13'43''$ |
| X–ray Peak | $12^h57^m26.2^s$ | $+28°12'28''$ |

Table 3: Coordinates of the four galaxies used to determine the image position of the component centres and the sky coordinates of NGC 4874 and the X–ray centre. the component centres.

the image coordinates were determined. The discrepancy between the two best calculations for each centre was found to be less than 20 pixels in either direction. The coordinates of the four reference galaxies, of NGC 4874, and of the X–ray gas (the X–ray peak in Ulmer *et al.* 1992) are given in Table 3.

### *4.3.2. Model Runs*

To pinpoint the best matching model, the simulations were used to map the four–parameter space (two semi-independent component percentages of the total number of data points to be simulated, and one dependent one, and two King profile core–radius values). The coordinates of the NGC 4874 GC population and IGC population centres were fixed at the coordinates specified in the previous subsection, as the former is easily determined as at the centre of the galaxy, and the latter is assumed to be associated with the centre of the X–ray gas distribution.

These assumptions are quite safe to take and were used to simplify the simulations significantly.

The initial run was used to create first a low–resolution map in all dimensions in order to reveal the region (or regions) where the lowest minima of $\bar{D}$ occur. Once this was determined, subsequent runs were operated with increasing resolution and numbers of averaged sub–runs to explore parameter space of decreasing size (around the region(s) of minimum $\bar{D}$), until the resolution is sufficiently fine.

The initial models were run with 30 averaged sub–runs, component percentage resolution of 5%, and core radius resolution of 100 pixels. The initial range of the parameters that were used were determined based on experience from test runs conducted prior to the simulations using artificial data and single–run "probing" simulations using the real data. The succeeding runs increased the percentage resolution to 1%, the NGC 4874 component core radius resolution to 5 pixels, and the X–ray gas component core radius to 50 pixels. In core radius–space, these values are beyond the optimum resolution, as the estimated uncertainties exceed these values. These uncertainties were also determined from the pre-simulation test runs. It was found that core radius uncertainty increases with increasing core radius, decreasing component fraction, and increasing number of overlapping components. At the large core radius region where the X-ray component core radius was determined to be, this uncertainty is approximately 150 pixels (about 70″) or more. For the smaller core radius region of the galaxy component, these are accurate to less than 50 pixels (about 24″). The statistics of the last set of models were calculated using one hundred sub–run statistics.

# 5. Results

## 5.1. Best – Fitting Model

Many models were examined with parameters which spanned significant ranges of values. As suggested by the results of the "probing" runs, the random background population was given compositions from 50% to 95%, the NGC 4874 component from 5% to 50%, and the IGC component from 0% to 90%, and both of the King-profile components were tested for core radii of 50 to 2500 pixels. The step sizes and number of "sub-runs" used were as described in Chapter 4.

The best-fitting model in this study was found to be composed of 81% random background; 18% NGC 4874 GCs, with a core radius of 475 pixels (approximately 3.7′); and 1% IGCs, with a core radius of 2250 pixels (approximately 18′). The KS $\bar{D}$-value of the match was 0.02945, corresponding to a significance level of 0.377 with the approximation in Press *et al.* (1992). The distribution of the model population is given in Figure 5.1, and a summary of the parametric and statistical results are given in Table 4.

## 5.2. Uncertainties of the Best – Fitting Model

The $1\sigma$ uncertainty in the value of $\bar{D}$ is $\pm 0.005$, obtained from the scatter of $\bar{D}$ among the sub-runs, which translates to about 200 pixels in the NGC 4874 component, 600 pixels in the IGC component, and 2% in the composition of the components. (These uncertainties were obtained by examining the parameters of the models which correspond to the $\bar{D}$ values at the extremities of the $\bar{D}$ uncertainty.) The uncertainties in the two King-type components' core radii are quite large

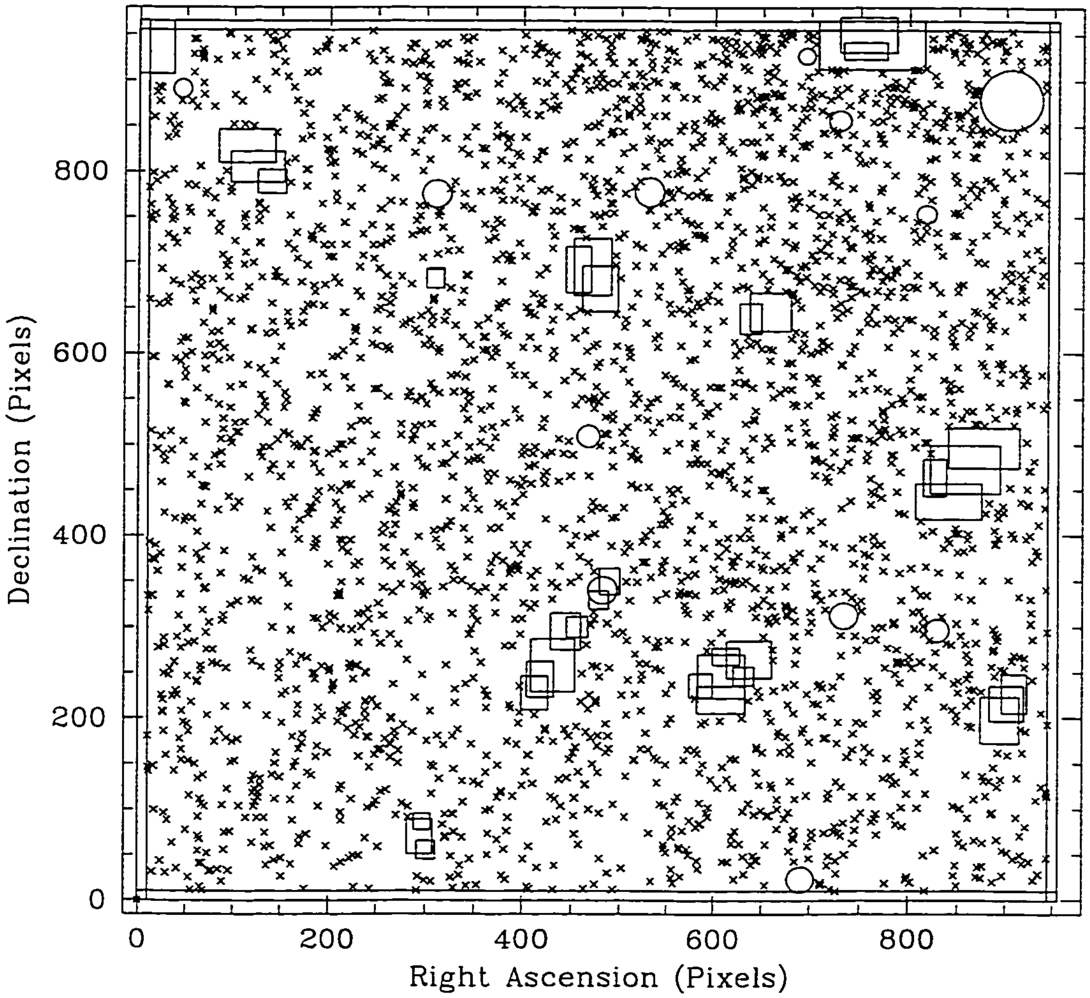


Fig. 5.1.— The distribution map of the best model for the Bea95 data. There are three components: a background, comprising 81% of the population, a population belonging to the galaxy, NGC 4874, with 18% composition and a core radius of 475 pixels (3.75′), and an IGC component centred on the X–ray centroid, with 1% composition and a core radius of 2250 pixels (18′).

mainly due to the very dominant background component. For the NGC 4874 GC component, this is because slight flattening or compacting (ie. slightly larger or smaller core radius, respectively) of this distribution is difficult for the program to distinguish from the best–fitting model because the large "flat" random background distribution overwhelms the smaller count of the NGC 4874 GC distribution and effectively hides minor changes in the distribution. As for the IGC component, it is because its distribution is already nearly as uniform as the background distribution, so a fairly large change in core radius does not alter the "flatness" too significantly.

As the test run results suggest for these ranges of values, however, the correct parameters of each component are very likely to fall within these uncertainties. Indeed, the core radii of the NGC 4874 and cluster X–ray components, as recorded by Vikhlinin *et al.* (1994), also listed in Table 4, both fall within the uncertainties of their respective best model core radius values. This implies that the GC distributions and the X–ray signatures of the cluster components both trace the respective component potentials. Conversely, the apparent association between the two sets of parameters further suggests that the conclusion that the correct parameters are within the $1\sigma$ uncertainty of the obtained parameters is probably correct and thus that we have effectively described the correct distribution.

### 5.3. Interpretation

If we consider the results of the program tests we conducted to test the effectiveness of the simulator program in addition to the results reported in the previous section, it is not difficult to accept that the parameters of the best–fitting model we created are probably very close to the actual values. If we also compare the

| | **Best Model** | | | **Obs. Data** | |
|---|---|---|---|---|---|
| | NGC 4874 | IGC | Background | NGC 4874 | X–ray |
| **Percent** | 18 | 1 | 81 | — | — |
| $\boldsymbol{R_c}$ **(pixels)** | 475 | 2250 | — | 313 | 1865 |
| $\boldsymbol{D}$ | $0.02945 \pm 0.005$ | | | — | |
| **Sig. Level** | 0.377 | | | — | |

Table 4: Listing of the parameters of the best matching model and the related statistics, compared to observational data. The observational core radius values are from Vikhlinin *et al.* 1994, and are both of the X–ray signatures of the components. Since Vikhlinin *et al.* (1994) lists the major and minor axes core radii of the cluster X–ray component, the value listed here is the average of the two values.

random background count of our best–fitting model and the corresponding Bea95 count of 74%, we can see that our count is in excess of the Bea95 count by 7%, which is greater than either of the background count uncertainties at the $1\sigma$ level. It is possible that this excess count actually belongs to the IGC component, and that the program interpreted these objects as belonging to the random background simply because of the flatness. Adding this excess count to the already detected IGC component would raise the IGC component population to 8% of the total number of Bea95 unresolved objects at this range of brightnesses, which would further suggest the existence of IGCs.

A great amount of caution must be exercised in any conclusions drawn here, however. At the $3\sigma$ level, the lower uncertainty of the NGC 4874 component core radius increases to 300 pixels and the upper increases to approximately 1000 pixels, while the uncertainties of the IGC component increase to more than 1500 pixels. In addition, the composition uncertainties increase to 7%, which puts Bea95's estimated background value into the model's uncertainty. This means that although we surely draw the conclusions stated above, we cannot eliminate the models whose goodness–of–fit results fall within the $3\sigma$ results, which certainly includes a large range of models.

In addition, at the $3\sigma$ level, the Bea95 background count uncertainty can account for the background count of the best–fitting model. At this level, the upper limit of the Bea95 count's uncertainty increases to 84.6%. This means, that, the excess 7%, and perhaps even the best–fit IGC 1% component, can still easily be interpreted as parts of the background distribution, the latter because its uncertainty, its flatness, and the results of program test 2 do not rule out the possibility of its being an illusion. This means that it is still very much possible that the detected IGCs do not exist.

Figure 5.2 displays a contour map of the KS test $\bar{D}$ values associated with combinations of background component composition and the core radius of the NGC 4874 component of the distribution. (Note that the value of $\bar{D}$ is mapped instead of the significance level. This is because, as mentioned in Chapter 3, the significance level may not be accurate above $\approx 0.20$.) In this map it can be seen that the region of minimum $\bar{D}$ is not an isolated locus, but is in fact a "stream" which leads from approximately $R_c \approx 250$ and background composition of 85% to $R_c \approx 65$ and composition of $\gg 2500$. The source of this "streaming" is, again, the confusion in data point possession. As the core radius of the model NGC 4874 component increases, more and more of the component's population lie farther and farther from the core. Because the central region of the galaxy component must maintain a

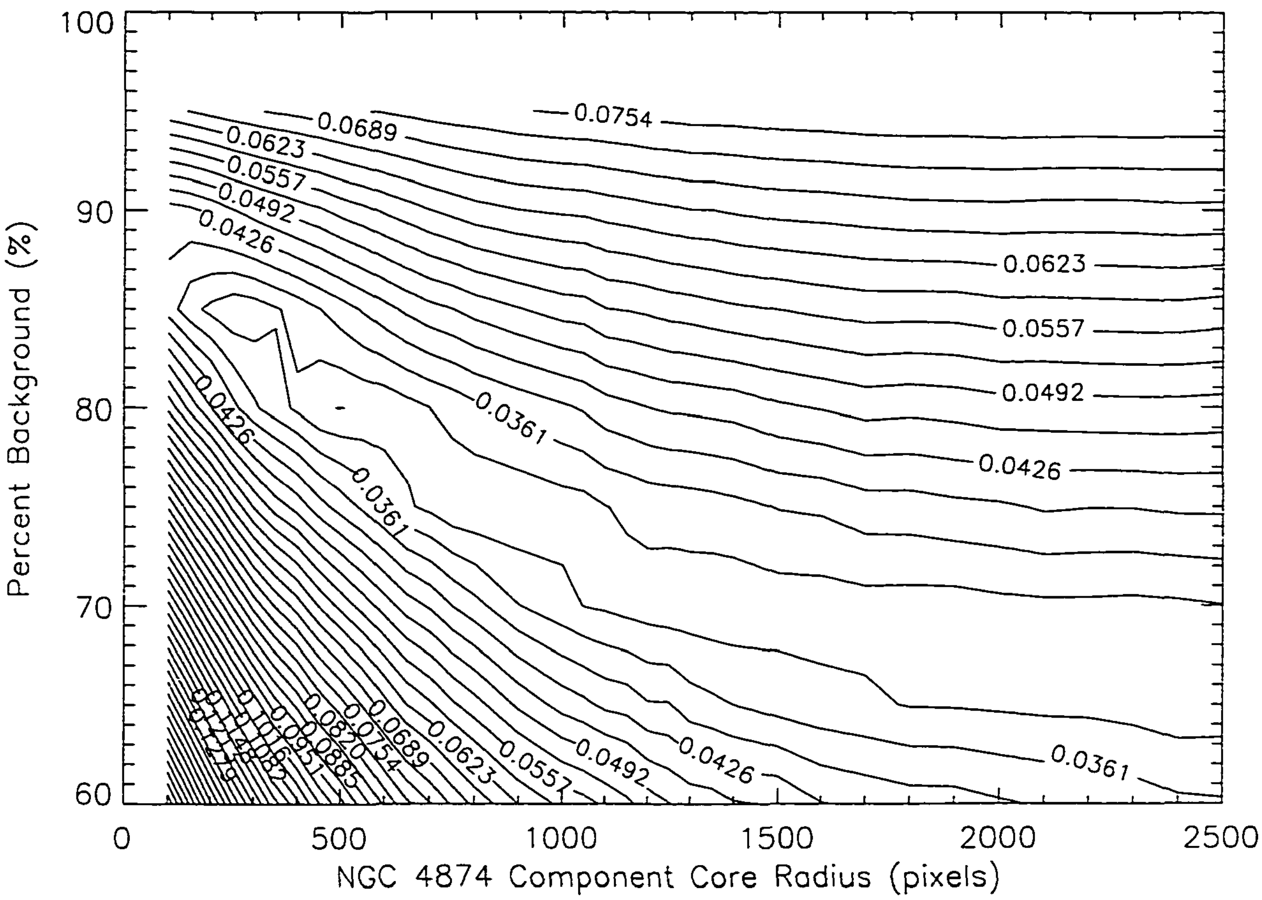


Fig. 5.2.— $\bar{D}$ level contours of the simulation models. The component percentage of the X–ray centroid component is held at 1% and the core radius is held at 2250 pixels. The kinks at 80 – 85% and core radii of 350 – 450 pixels are artifacts of the low-resolution of the mapping.

certain amount of population to match the real data, it requires more population to boost the central region to compensate for the spreading out of the data points, and this must occur at the cost of the background component population, which drops with increasing galaxy component core radius. Because at large galaxy component core radius, the outer part of the component become very flat, it becomes difficult to distinguish from the background component, and hence mimics the true distribution very well and produces similarly low $\bar{D}$ values. Although this scenario does explain the "stream" very well, it does not exclude any of the models within the "stream" from suspicion as being the correct one. So, again, caution must be made in our conclusions.

## 5.4. Additional Uncertainties

### *5.4.1. Uncertainty in the Background Counts*

There is an additional caveat to a claim that the best model is indeed the one which describes the Coma distribution the best. A recent study by Adami *et al.* (1998, see also Secker *et al.* 1997) indicates that the Bea95 background counts may, in fact, be underestimated. In their study Adami *et al.* took spectroscopic measurements of 34 galaxies within the Bea95 Coma Cluster field at about $R \approx 22$ and found that almost all of the galaxies detected by Bea95 in that magnitude region in fact belong to a "physical structure" at $z \approx 0.5$ (compared to $z \approx 0.023$ for Coma). If so, then the background field counts of the Bea95 Coma field cannot be compared to that of the control fields, and thus the Bea95 background counts are probably considerably underestimated. This means that the true background counts might actually account for the entire population of background data points detected in our study, barring the existence of IGCs.

We also conducted a small investigation into the possible undercounting of background galaxies by Bea95. Comparing the Metcalfe *et al.* (1991) parametrization of background galaxy counts:

$$log N_{gal} = 0.37R - 4.2, \tag{5.1}$$

where $R$ is the red magnitude, and $N_{gal}$ is the number of galaxies per square degree per unit magnitude interval. This translates to:

$$\frac{dN_{gal}}{dL} \propto L^{-1.9}, \tag{5.2}$$

where $L$ is the luminosity of the galaxies. It can be seen that this luminosity function of faint background sources has a slope which is comparable to that of the Bea95 unresolved objects. This suggests that perhaps the Bea95 background reduction did not effectively eliminate the background galaxy contamination after all, and that a significant additional number from the remainder of the objects (after background reduction) are indeed background galaxies, perhaps accounting for all the remaining 7% of the background count of the best–fitting model.

To test this possibility we divided the Bea95 data into two nearly even halves, and tested their goodness–of–fit to each other using the 2DKS test alone. The Bea95 paper suggests that the object and background galaxy counts in the two halves should be very similar to each other. It was found, however, that they match only at the 8% confidence level. (Note that this value is within the reliable limit of the calculation of the confidence level for this version of the test.) This means that the two halves are statistically similar, although barely so.

We then created models for each half, and tested it using the same model–and–test method as before. We found that the test for the brighter half assigns more of the unresolved objects to the NGC 4874 population (from 18% to 27%) and the test for the dimmer half assigns more of them to the background counts (from 81% to 83%). The percentage population and the core radius of the IGC component remained approximately the same. The core radius of the NGC 4874 component increased to 710 pixels for the brighter half, and 630 for the dimmer half. The core radii here are larger than that of the best–fitting model probably because the sample sizes are smaller, so it is more difficult to distinguish between the outer members of the King–profile components and the random background component. The simplest explanation for population count changes is that the number of the background galaxies rises faster than that of the GCs (recall that we only have the brighter luminosity tail of the GC luminosity function here), so that at the dimmer half of the Bea95 data the GCs is diluted more by background galaxies than at the brighter half. This implies that the Bea95 count is probably underestimated, more so at the lower luminosity end, as the Bea95 background counts predict that counts of both halves should be very comparable.

### *5.4.2. Uncertainty in the Centroids*

One more possible source of uncertainty was also investigated, and that is the possibility that the coordinates of the centres of the distributions are incorrect and thus may influence the statistical calculations. It has been noted from trial runs that the 2DKS test is highly sensitive to mispositioning, so this problem is not a trivial one. To check this possibility, a test was conducted whereby the central coordinates of the galaxy component were varied slightly (the IGC component is not considered because it is flat enough that it is almost indistinguishable from the background component, and thus a slight change of central coordinates should not affect the results significantly enough). The coordinates were changed $\pm 10$ pixels and $\pm 30$ pixels in both directions and combinations thereof (including with the central coordinate of each direction), and a set of models were tested for goodness–of–fit at each coordinate combination. It was found that there is considerable variation in goodness–of–fit with the coordinate change, but it was found that the original coordinates nevertheless belong to the best–fitting model, so we conclude that the coordinate pair we use for the centre of the galaxy distribution is at, or is very close to, the correct one.

## 5.5. Object "Stream" SW of NGC 4874

It must also be noted that in the northwestern corner of the Bea95 distribution, just southwest of the position of NGC 4874 there is a very noticable swath of objects from approximately the position on NGC 4874 through the masked–out galaxy, NGC 4872, to its southwest and proceeding slightly farther to the southwest. (Compare Figures 2.4 and 5.1. Note that NGC 4874 is just to the northeast of the object masked by the rectangles on the right of the upper edge of the image, so this swath of objects clearly does not belong exclusively to NGC 4874's GC population.) Although the exact position of NGC 4874 with respect to the image has some associated uncertainty, the position of this group of objects is too extended only in one direction (to the southwest) to belong to a purely King–profile NGC 4874 distribution, and our best model distribution confirms this, indicating that it is probably an extraneous feature. The X–ray maps in Vikhlinin (1994) shows that there is a slight extension of the X–ray gas pointing to the south–southwest, so it is possible that these objects are a stream of GCs which also traces the mass distribution that the X–ray gas does. The origin and implications of this phenomenon is certainly worth investigating.

### 5.6. Summary of Results

With the uncertainties outlined above, it is not easy to conclude beyond any shadow of a doubt that we have indeed found the correct distribution of the Bea95 objects. It is true, however, that we have clearly established some conditions which further models of IGCs must meet in order to be acceptable. The parameter space "stream" that we detected (see Figure 5.2) has considerable length, but it is nevertheless very narrow within the $1\sigma$ level. This means that within these limits, only distribution models with these combinations of percentage composition and King–profile–component core radii can be considered. If one can believe that our best–model is indeed the correct one, then any composition model must account for a non–galaxy (NGC 4874) component which is composed of an 82% (including the detected IGC component) population of flatly distributed objects.

However, given the reliability of our method as demonstrated by our tests on simulated data, and the fact that our best–fit model seems to effectively trace the distribution of the cluster X–ray signatures, it seems reasonable to conclude that our best–fitting model is likely to be close to the true distribution of faint objects in Coma. Whether the expected number of "background" objects that we detected is indicative of a bona fide IGC population, or merely an underestimate of background galaxy contamination by Bea95, will require more and better data covering a larger area of the Coma core region. For now, we can only say that, although we do not rule out the models which fall within the “stream” in parameter space, nor models which do not include IGCs, there is some possibility that IGCs may exist.

## 6. Conclusion

In this study we have attempted to discover whether there exist globular clusters which belong only to the Coma Cluster's gravitational potential well. We developed and tested a method of searching for IGCs, and showed that it is a sensitive diagnostic tool. We then applied our methodology to a catalogue of unresolved objects from the Bernstein *et al.* (1995) study and endeavoured to model their distribution in order to learn if a model with an intracluster globular cluster component can effectively describe this distribution. We tested the similarity between each model and the Bea95 distribution using a two–dimensional, two–sample version of the sensitive Kolmogorov–Smirnov test of goodness–of–fit.

We have found that the best–fitting model is composed of an 81% random background component, an 18% NGC 4874 GC component in a King–type distribution with a core radius of approximately 3.7′, and a 1% IGC component in a King–type distribution with a core radius of approximately 18′. With the Bea95 background count of 74%, this means that as much as 8% of the population potentially belongs to an IGC component, since the IGC component is so flatly distributed that the unaccounted for 7% excess background count may in fact belong to the IGC distribution. Since the distribution found seems to also reflect the X–ray observations of Vikhlinin *et al.* (1994), and the tests of the method show favourably its effectiveness, they suggest that, within the uncertainties, we have indeed found the correct distribution of the Bea95 objects, and that IGCs may exist.

However, there remains a significant amount of uncertainty in the data and in the results, so we can claim nothing very conclusive about the existence of IGCs. The range of acceptably–fitting models is too extensive to surely eliminate many of the models, and a recent investigation into the background counts within the Bea95 work revealed that their counts are probably underestimated, and hence may account for all of our detected background count, and even perhaps our IGC count.

In order to improve the results of this line of investigation, it is first and foremost important that better data be obtained. The resolution of the Bea95 data was, first of all, insufficient for separating GCs from other objects within the Coma core and background contaminants. Higher resolution images from telescopes such as the Hubble Space Telescope or CFHT may be required in order to "clean" the data to obtain less uncertain conclusions about the results of this test.

To improve model fits and provide more reliable statistics, it is also prudent that a larger, more complete field of the Coma cluster core is obtained. This would increase the object counts and create a more complete picture of the distributions, hence increasing the sample size and preventing erronous results due to fitting partial distributions. Furthermore, it would allow the detection of the radial density fall–off of the IGC distribution, so that the models can be much better fitted and constrained.

To be more thorough, it is also recommended that parameters fixed in this study, namely, the positions of the centres of the King–profile distributions, are treated also as free parameters. Although this would increase computation time, it would give the method more freedom to find the correct parameters to a higher degree, thus improving the beliveability of the results and decreasing some of the uncertainties.

Finally, since the KS test is only one of several reliable tests of goodness–of–fit, it is perhaps a good idea to also attempt this method using other, similarly reliable tests, such as the $\chi^2$ test. Even if such a test reveals the same results as that of the KS test, it could serve as proof that the two–dimensional KS test is just as reliable in this usage.

# Appendix

This is the FORTRAN code used for the simulation runs. The descriptions of the functions of certain sections are listed within the code below, and the procedures for running the program is described within the text.

```
      PROGRAM PEPPER

C This program takes an observed two-dimensional distribution and
C compares it with theoretical distributions using the two--
C dimensional Kolmogorov-Smirnov (hereafter KS) test. The program is
C capable of creating models of several components to be combined.
C Presently it is fitted with these component distributions:
C   1. Random distribution (e.g. for background distributions),
C   2. King (1962) profile distribution, and
C It is also capable of using data from images (etc.) with masked
C and deleted sections with a subroutine which specifies the sections
C to be ignored. The models are (can be) averaged to smoothe out
C statistical fluctuations. The random number generator and the KS
C subroutines were obtained from Press et al. (1992) with minor
C changes. The KS D parameter for all models are reported as well as
C the coordinates of the best model data points.

      INTEGER   COMP, NUMGC, CTRF, CTRL0, CTRL1, CTRL2, CUT, SEED
      INTEGER   CTRL3, CTRL4, J, K, L, M, N, P, Q, GCCT, COMPCT
      INTEGER   RUNNUM, NIT, KOLD
      INTEGER   GCN(1000), DIST(1000), SLST(100)
      REAL      PERSUM, XSIZE, YSIZE
      REAL      D, DPRIME, DOLD, ZED, ZEDPR, ZOLD, PROB, POLD
      REAL      CENX(1000), CENY(1000), PERCNT(1000), RC(1000)
      REAL      CLX(100000), CLY(100000), COX(100000), COY(100000)
      REAL      COTX(100000), COTY(100000), PEROLD(1000), RCOLD(1000)

C Open the necessary files. ComaGC.txt is the input data file,
C Input.bat is the parameter input file, Master.txt is the output
C coordinate file (for the best match only), and Result.dat is the
C output data file (the relevant parameters for all the runs).

      OPEN (UNIT = 50, FILE = 'Master.txt', STATUS = 'NEW')
      OPEN (UNIT = 60, FILE = 'ComaGCt.txt', STATUS = 'OLD')
      OPEN (UNIT = 70, FILE = 'Input.bat', STATUS = 'OLD')
      OPEN (UNIT = 80, FILE = 'Result.dat', STATUS = 'NEW')

C The number of models, the choice of including deleted sections,
C the number of iterations to be averaged, and the number of input
C data points included in the calculations are read from the
C Input.bat file. Then the data coordinates are read from the
```

```
C ComaGC.txt file, then the seed values for the to-be-averaged
C sub-runs.

      READ (70, *) RUNNUM, CUT, NIT, NUMGC
      DOLD = 100.
      ZOLD = 100.
      DO 10 J = 1, NUMGC, 1
         READ (60, *) COX(J), COY(J)
 10   CONTINUE
      DO 15 M = 1, NIT, 1
         READ (70, *) SLST(M)
 15   CONTINUE

C The program creates RUNNUM number of models. It begins by reading
C the number of components and the size of the region to be modeled
C from the Input.bat file. It then reads the component parameters
C (the distribution type, the centre of the distribution (read 0 if
C background), and the percent amount of the total number of data
C points the component comprises. The core radius (or related para-
C meter) (again, defined as 0 for background, and not used) is then
C read and the percent values are recalculated as decimal values.
C The number of globular clusters to be produced in each model com-
C ponent is calculated.

      DO 90 K = 1, RUNNUM, 1
        PERSUM = 0
        DPRIME = 0
        ZEDPR = 0
        READ (70, *) COMP, XSIZE, YSIZE
        DO 20 CTRL1 = 1, COMP, 1
           READ (70, *) DIST(CTRL1), CENX(CTRL1), CENY(CTRL1),
     +                  PERCNT(CTRL1)
           IF ((DIST(CTRL1).EQ.2).OR.(DIST(CTRL1).EQ.3)) THEN
              READ (70, *) RC(CTRL1)
           ELSE
              RC(CTRL1) = 0
           ENDIF
           IF (CTRL1 .LE. COMP - 1) THEN
              PERCNT(CTRL1) = PERCNT(CTRL1) / 100
           ENDIF
 20     CONTINUE
        IF (COMP .GT. 1) THEN
           DO 50 CTRL2 = 1, (COMP - 1), 1
              PERSUM = PERSUM + PERCNT(CTRL2)
 50        CONTINUE
           PERCNT(COMP) = 1 - PERSUM
           IF ((PERCNT(CTRL1) .LT. 0) .AND. (COMP .NE. 1)) THEN
              PRINT *,'Your total percentage is more than 100%,
     +                please enter component data again.'
              STOP
           ENDIF
```

```
            DO 70 CTRL3 = 1, COMP, 1
               GCN(CTRL3) = NUMGC * PERCNT(CTRL3)
70          CONTINUE
         ELSE
            GCN(1) = NUMGC
         ENDIF

C Each model is run NIT times and the D and Z' values are averaged.
C For each component the appropriate subroutine for the distribution
C type is called, each contributing to the output coordinate file
C if used. Each sub-model is tested with the KS tester and the
C results are reported in the Result.dat file.

         DO 74 L = 1, NIT, 1
           CTRL0 = 0
           SEED = - SLST(L)
           DO 72 CTRL4 = 1, COMP, 1
              IF (DIST(CTRL4) .EQ. 1) CALL BACK(CUT, SEED, CTRL0,
     +                L, NIT, CTRL4, XSIZE, YSIZE, GCN, CLX, CLY)
              IF (DIST(CTRL4) .EQ. 2) CALL KING(CUT, SEED, CTRL0,
     +                    L, NIT, CTRL4, XSIZE, YSIZE, GCN, CENX,
     +                                 CENY, CLX, CLY, RC(CTRL4))
 72        CONTINUE
           PRINT *,'Simulation number ', K, ' is complete.'
           DO CTRF = 1, COMP, 1
             PRINT *,'The number of globular clusters in component',
     +               CTRF, ' is', GCN(CTRF)
           ENDDO
           PRINT *,' '
           PRINT *,'Total number of globular clusters is ', CTRL0
           CALL KS2D2S(COX, COY, NUMGC, CLX, CLY, CTRL0, D, ZED,
     +                 PROB)
           IF (D .LE. 0.15) WRITE (80, 79) K, L, D, ZED, PROB
           DPRIME = DPRIME + D
           ZEDPR = ZEDPR + ZED
 74      CONTINUE

C The averaged D and Z' values are reported, and if the latest ave
C raged D value is less than the previous, then the coordinates of
C the last sub-model is saved into temporary coordinate variables.
C The input parameters for the model are also reported in the
C Result.dat file, along with the D, Z', and signifivance level
C values. The best matching model parameters are also rereported in
C the Result.dat file after a space.

         D = DPRIME / FLOAT(NIT)
         ZED = ZEDPR / FLOAT(NIT)
         PROB = PROBKS(ZED)
         WRITE (80, 80) K, D, ZED, PROB
         IF (D .LT. DOLD) THEN
            DO 75 Q = 1, COMP, 1
```

```
            PEROLD(Q) = PERCNT(Q)
            RCOLD(Q) = RC(Q)
   75     CONTINUE
          DOLD = D
          ZOLD = ZED
          POLD = PROB
          KOLD = K
          DO 76 P = 1, NUMGC, 1
             COTX(P) = CLX(P)
             COTY(P) = CLY(P)
   76     CONTINUE
        ENDIF
        DO 78 N = 1, COMP, 1
           WRITE (80, 85) DIST(N), PERCNT(N), RC(N)
   78   CONTINUE
        CALL FLUSH(80)

   79   FORMAT (I5, 2X, I2, 2X, F14.10, 2X, F14.10, 2X, E12.6)
   80   FORMAT (I5, 2X, F12.10, 2X, F14.10, 2X, E12.6)
   85   FORMAT (I5, 2X, F7.5, 2X, F7.1)

   90 CONTINUE
      WRITE (80, *) ' '
      WRITE (80, 98) KOLD, DOLD, ZOLD, POLD
      DO 91 COMPCT = 1, COMP, 1
         WRITE (80, 97) COMPCT, PEROLD(COMPCT), RCOLD(COMPCT)
   91 CONTINUE

C The coordinates for the best-matching model is saved into the
C Master.txt file.

      DO 92 GCCT = 1, NUMGC, 1
         WRITE (50, 95) COTX(GCCT), COTY(GCCT)
   92 CONTINUE

   95 FORMAT (F12.5, 2X, F12.5)
   97 FORMAT (I5, 2X, F7.5, 2X, F7.1)
   98 FORMAT (I5, 2X, F12.10, 2X, F14.10, 2X, E12.6)
      CLOSE (UNIT = 50)
      CLOSE (UNIT = 80)
      PRINT *,'The calculations are complete!'

      STOP
      END

*******************************************************************

      SUBROUTINE BACK(CUT, SEED, CTRL0, L, NIT, CTRL4, XSIZE,
     +                                   YSIZE, GCN, CLX, CLY)

C Computes a random "background" distribution limited by the
```

```
C boundaries of the model.

      INTEGER   CTRL0, CTRL4, CTRL5, CTRL9, SEED, CUT, NIT, L
      INTEGER   GCN(30)
      REAL      X, Y, XSIZE, YSIZE, CLX(100000), CLY(100000)

      CTRL5 = 1
      DO WHILE (CTRL5 .LE. GCN(CTRL4))
         X = XSIZE * RA(SEED)
         Y = YSIZE * RA(SEED)
         IF (CUT .EQ. 1) THEN
            CALL CUTOUT(X, Y, CTRL5, CTRL9)
            IF (CTRL9 .EQ. CTRL5) THEN
               CLX(CTRL0) = X
               CLY(CTRL0) = Y
               CTRL0 = CTRL0 + 1
            ELSE
               CTRL5 = CTRL5 - 1
            ENDIF
         ELSE
            CLX(CTRL0) = X
            CLY(CTRL0) = Y
            CTRL0 = CTRL0 + 1
         ENDIF
         CTRL5 = CTRL5 + 1
      ENDDO
      PRINT *,'Component ', CTRL4,' calculation complete.'

      RETURN
      END

******************************************************************

      SUBROUTINE KING(CUT, SEED, CTRL0, L, NIT, CTRL4, XSIZE,
     +                 YSIZE, GCN, CENX, CENY, CLX, CLY, RC)

C Computes a randomly-generated King-profile distribution centred
C at XCORR, YCORR, with core radius RC, limited by the boundaries
C of the model. If the generated coordinates are outside the
C boundaries, it is recalculated.

      REAL      PI
      PARAMETER (PI = 3.141592654)
      INTEGER   CTRL0, CTRL4, CTRL6, CTRL9, SEED, CUT, NIT, L
      INTEGER   GCN(1000)
      REAL      R, RC, THETA, X, XCORR, YCORR, Y, XSIZE, YSIZE
      REAL      CENX(1000), CENY(1000), CLX(100000), CLY(100000)

      CTRL6 = 1
      DO WHILE (CTRL6 .LE. GCN(CTRL4))
         THETA = 2 * PI * RA(SEED)
```

```
         R = RC * TAN(PI * RA(SEED) / 2)
         X = R * COS(THETA)
         Y = R * SIN(THETA)
         XCORR = X + CENX(CTRL4)
         YCORR = Y + CENY(CTRL4)
         IF ((XCORR .GT. XSIZE) .OR. (XCORR .LT. 0) .OR.
     +       (YCORR .GT. YSIZE) .OR. (YCORR .LT. 0)) THEN
            CTRL6 = CTRL6 - 1
         ELSE IF (CUT .EQ. 1) THEN
            CALL CUTOUT(XCORR, YCORR, CTRL6, CTRL9)
            IF (CTRL9 .EQ. CTRL6) THEN
               CLX(CTRL0) = XCORR
               CLY(CTRL0) = YCORR
               CTRL0 = CTRL0 + 1
            ELSE
               CTRL6 = CTRL6 - 1
            ENDIF
         ELSE
            CLX(CTRL0) = XCORR
            CLY(CTRL0) = YCORR
            CTRL0 = CTRL0 + 1
         ENDIF
      CTRL6 = CTRL6 + 1
      ENDDO
      PRINT *,'Component ', CTRL4,' calculation complete.'

      RETURN
      END

******************************************************************

C     Using function "ran3" from Press et al (1992),
C     Chapter 7.1, a random number generator.

      REAL FUNCTION RA(SEED)

      INTEGER   SEED
      INTEGER   MBIG, MSEED, MZ
      REAL      RA, FAC
      PARAMETER (MBIG=1000000000, MSEED=161803398, MZ=0, FAC=1./MBIG)
      INTEGER   I, IFF, II, INEXT, INEXTP, K
      INTEGER   MJ, MK, MA(55)

      SAVE IFF, INEXT, INEXTP, MA
      DATA IFF /0/

      IF (SEED .LT. 0 .OR. IFF .EQ. 0) THEN
         IFF = 1
         MJ = MSEED - IABS(SEED)
         MJ = MOD(MJ,MBIG)
         MA(55) = MJ
```

```
          MK = 1
          DO 411 I = 1, 54
             II = MOD(21 * I, 55)
             MA(II) = MK
             MK = MJ - MK
             IF (MK .LT. MZ) MK = MK + MBIG
             MJ = MA(II)
  411     CONTINUE
          DO 413 K = 1, 4
             DO 412 I = 1, 55
                MA(I) = MA(I) - MA(1 + MOD(I+30, 55))
                IF (MA(I) .LT. MZ) MA(I) = MA(I) + MBIG
  412        CONTINUE
  413     CONTINUE
          INEXT = 0
          INEXTP = 31
          SEED = 1
       ENDIF
       INEXT = INEXT + 1
       IF (INEXT .EQ. 56) INEXT = 1
       INEXTP = INEXTP + 1
       IF (INEXTP .EQ. 56) INEXTP = 1
       MJ = MA(INEXT) - MA(INEXTP)
       IF (MJ .LT. MZ) MJ = MJ + MBIG
       MA(INEXT) = MJ
       RA = MJ * FAC

       RETURN
       END

******************************************************************

       SUBROUTINE CUTOUT(XCORR, YCORR, CTRL10, CTRL11)

C The subroutine for accounting for the masked and deleted sections
C of the real data. The "R" calculations account for the circular
C cuts, and the remainder accounts for the rectangular cuts. Each
C distribution subroutine may call this subroutine, which acts as
C "inner boundaries" for the model. If a data point falls within the
C specified limits, it is recalculated. It functions by comparing the
C values of "CTRL10" and "CTRL11". If they match, then the point is
C counted, otherwise it is rejected. The defined value of "CTRL11" if
C the point falls within the region is arbitrary, as long as it takes
C a value that "CTRL10" will never have.

       INTEGER CTRL10, CTRL11
       REAL    XCORR, YCORR
       REAL    R1, R2, R3, R4, R5, R6, R7, R8, R9, R10, R11, R12

       CTRL11 = CTRL10
```

```
      R1 = SQRT((467. - XCORR)**2 + (509. - YCORR)**2)
      R2 = SQRT((45. - XCORR)**2 + (891. - YCORR)**2)
      R3 = SQRT((310. - XCORR)**2 + (775. - YCORR)**2)
      R4 = SQRT((530. - XCORR)**2 + (777. - YCORR)**2)
      R5 = SQRT((817. - XCORR)**2 + (753. - YCORR)**2)
      R6 = SQRT((482. - XCORR)**2 + (340. - YCORR)**2)
      R7 = SQRT((691. - XCORR)**2 + (23. - YCORR)**2)
      R8 = SQRT((829. - XCORR)**2 + (296. - YCORR)**2)
      R9 = SQRT((734. - XCORR)**2 + (312. - YCORR)**2)
      R10 = SQRT((729. - XCORR)**2 + (856. - YCORR)**2)
      R11 = SQRT((695. - XCORR)**2 + (927. - YCORR)**2)
      R12 = SQRT((905. - XCORR)**2 + (879. - YCORR)**2)
      IF (R1 .LE. 12.) CTRL11 = -5
      IF (R2 .LE. 10.) CTRL11 =  -5
      IF (R3 .LE. 15.) CTRL11 = -5
      IF (R4 .LE. 16.) CTRL11 =  -5
      IF (R5 .LE. 10.) CTRL11 =  -5
      IF (R6 .LE. 15.) CTRL11 =  -5
      IF (R7 .LE. 14.) CTRL11 =  -5
      IF (R8 .LE. 12.) CTRL11 =  -5
      IF (R9 .LE. 14.) CTRL11 =  -5
      IF (R10 .LE. 11.) CTRL11 =  -5
      IF (R11 .LE. 9.) CTRL11 =  -5
      IF (R12 .LE. 33.) CTRL11 =  -5
      IF ((XCORR .GE. 451.) .AND. (XCORR .LE. 490.) .AND.
     +  (YCORR .GE. 664.) .AND. (YCORR .LE. 726.)) CTRL11 = -5
      IF ((XCORR .GE. 460.) .AND. (XCORR .LE. 497.) .AND.
     +  (YCORR .GE. 646.) .AND. (YCORR .LE. 696.)) CTRL11 = -5
      IF ((XCORR .GE. 443.) .AND. (XCORR .LE. 469.) .AND.
     +  (YCORR .GE. 667.) .AND. (YCORR .LE. 717.)) CTRL11 = -5
      IF ((XCORR .GE. 637.) .AND. (XCORR .LE. 680.) .AND.
     +  (YCORR .GE. 625.) .AND. (YCORR .LE. 667.)) CTRL11 = -5
      IF ((XCORR .GE. 627.) .AND. (XCORR .LE. 649.) .AND.
     +  (YCORR .GE. 622.) .AND. (YCORR .LE. 655.)) CTRL11 = -5
      IF ((XCORR .GE. 96.) .AND. (XCORR .LE. 153.) .AND.
     +  (YCORR .GE. 788.) .AND. (YCORR .LE. 822.)) CTRL11 = -5
      IF ((XCORR .GE. 84.) .AND. (XCORR .LE. 143.) .AND.
     +  (YCORR .GE. 810.) .AND. (YCORR .LE. 846.)) CTRL11 = -5
      IF ((XCORR .GE. 125.) .AND. (XCORR .LE. 155.) .AND.
     +  (YCORR .GE. 776.) .AND. (YCORR .LE. 802.)) CTRL11 = -5
      IF ((XCORR .GE. 300.) .AND. (XCORR .LE. 318.) .AND.
     +  (YCORR .GE. 672.) .AND. (YCORR .LE. 693.)) CTRL11 = -5
      IF ((XCORR .GE. 822.) .AND. (XCORR .LE. 894.) .AND.
     +  (YCORR .GT. 446.) .AND. (YCORR .LT. 499.)) CTRL11 = -5
      IF ((XCORR .GE. 807.) .AND. (XCORR .LE. 875.) .AND.
     +  (YCORR .GE. 418.) .AND. (YCORR .LE. 457.)) CTRL11 = -5
      IF ((XCORR .GE. 840.) .AND. (XCORR .LE. 915.) .AND.
     +  (YCORR .GE. 474.) .AND. (YCORR .LE. 518.)) CTRL11 = -5
      IF ((XCORR .GE. 815.) .AND. (XCORR .LE. 838.) .AND.
     +  (YCORR .GE. 443.) .AND. (YCORR .LE. 484.)) CTRL11 = -5
      IF ((XCORR .GE. 281.) .AND. (XCORR .LE. 308.) .AND.
```

```
+  (YCORR .GE. 51.) .AND. (YCORR .LE. 89.)) CTRL11 = -5
   IF ((XCORR .GE. 288.) .AND. (XCORR .LE. 306.) .AND.
+  (YCORR .GE. 77.) .AND. (YCORR .LE. 95.)) CTRL11 = -5
   IF ((XCORR .GE. 291.) .AND. (XCORR .LE. 311.) .AND.
+  (YCORR .GE. 45.) .AND. (YCORR .LE. 65.)) CTRL11 = -5
   IF ((XCORR .GE. 409.) .AND. (XCORR .LE. 453.) .AND.
+  (YCORR .GE. 229.) .AND. (YCORR .LE. 287.)) CTRL11 = -5
   IF ((XCORR .GE. 405.) .AND. (XCORR .LE. 432.) .AND.
+  (YCORR .GE. 223.) .AND. (YCORR .LE. 262.)) CTRL11 = -5
   IF ((XCORR .GE. 399.) .AND. (XCORR .LE. 426.) .AND.
+  (YCORR .GE. 209.) .AND. (YCORR .LE. 246.)) CTRL11 = -5
   IF ((XCORR .GE. 429.) .AND. (XCORR .LE. 459.) .AND.
+  (YCORR .GE. 275.) .AND. (YCORR .LE. 315.)) CTRL11 = -5
   IF ((XCORR .GE. 445.) .AND. (XCORR .LE. 467.) .AND.
+  (YCORR .GE. 289.) .AND. (YCORR .LE. 311.)) CTRL11 = -5
   IF ((XCORR .GE. 479.) .AND. (XCORR .LE. 500.) .AND.
+  (YCORR .GE. 335.) .AND. (YCORR .LE. 364.)) CTRL11 = -5
   IF ((XCORR .GE. 468.) .AND. (XCORR .LE. 488.) .AND.
+  (YCORR .GE. 319.) .AND. (YCORR .LE. 339.)) CTRL11 = -5
   IF ((XCORR .GE. 583.) .AND. (XCORR .LE. 633.) .AND.
+  (YCORR .GE. 222.) .AND. (YCORR .LE. 270.)) CTRL11 = -5
   IF ((XCORR .GE. 582.) .AND. (XCORR .LE. 633.) .AND.
+  (YCORR .GE. 205.) .AND. (YCORR .LE. 235.)) CTRL11 = -5
  IF ((XCORR .GE. 614.) .AND. (XCORR .LE. 661.) .AND.
+  (YCORR .GE. 244.) .AND. (YCORR .LE. 285.)) CTRL11 = -5
   IF ((XCORR .GE. 574.) .AND. (XCORR .LE. 599.) .AND.
+  (YCORR .GE. 223.) .AND. (YCORR .LE. 249.)) CTRL11 = -5
   IF ((XCORR .GE. 621.) .AND. (XCORR .LE. 642.) .AND.
+  (YCORR .GE. 236.) .AND. (YCORR .LE. 256.)) CTRL11 = -5
   IF ((XCORR .GE. 599.) .AND. (XCORR .LE. 628.) .AND.
+  (YCORR .GE. 258.) .AND. (YCORR .LE. 277.)) CTRL11 = -5
   IF ((XCORR .GE. 874.) .AND. (XCORR .LE. 915.) .AND.
+  (YCORR .GE. 172.) .AND. (YCORR .LE. 223.)) CTRL11 = -5
   IF ((XCORR .GE. 896.) .AND. (XCORR .LE. 923.) .AND.
+  (YCORR .GE. 205.) .AND. (YCORR .LE. 248.)) CTRL11 = -5
   IF ((XCORR .GE. 884.) .AND. (XCORR .LE. 920.) .AND.
+  (YCORR .GE. 196.) .AND. (YCORR .LE. 235.)) CTRL11 = -5
   IF ((XCORR .GE. 729.) .AND. (XCORR .LE. 787.) .AND.
+  (YCORR .GE. 931.) .AND. (YCORR .LE. 969.)) CTRL11 = -5
   IF ((XCORR .GE. 733.) .AND. (XCORR .LE. 777.) .AND.
+  (YCORR .GE. 923.) .AND. (YCORR .LE. 942.)) CTRL11 = -5
   IF ((XCORR .GE. 0.) .AND. (XCORR .LE. 955.) .AND.
+  (YCORR .GE. 0.) .AND. (YCORR .LE. 10.)) CTRL11 = -5
   IF ((XCORR .GE. 0.) .AND. (XCORR .LE. 10.) .AND.
+  (YCORR .GT. 0.) .AND. (YCORR .LT. 965.)) CTRL11 = -5
   IF ((XCORR .GE. 0.) .AND. (XCORR .LE. 955.) .AND.
+  (YCORR .GE. 955.) .AND. (YCORR .LE. 965.)) CTRL11 = -5
   IF ((XCORR .GE. 945.) .AND. (XCORR .LE. 955.) .AND.
+  (YCORR .GE. 0.) .AND. (YCORR .LE. 965.)) CTRL11 = -5
   IF ((XCORR .GE. 0.) .AND. (XCORR .LE. 36.) .AND.
+  (YCORR .GE. 907.) .AND. (YCORR .LE. 965.)) CTRL11 = -5
```

```
      IF ((XCORR .GE. 707.) .AND. (XCORR .LE. 815.) .AND.
     +  (YCORR .GE. 912.) .AND. (YCORR .LE. 965.)) CTRL11 = -5

      RETURN
      END
```

```
*******************************************************************

      SUBROUTINE KS2D2S(X1, Y1, N1, X2, Y2, N2, D, ZED, PROB)

C The two-dimensional, two sample Kolmogorov-Smirnov test routine
C from Chapter 14.7 of Press et al. (1992), along with its support
C subroutines. It has been slightly modified to exclude the calcu-
C lation of unneeded parameters.

      INTEGER N1, N2
      REAL    D, ZED, PROB, X1(N1), X2(N2), Y1(N1), Y2(N2)
      INTEGER J
      REAL    D1, D2, FA, FB, FC, FD, GA, GB, GC,
     *        GD, R1, R2, RR, SQEN, PROBKS

      D1 = 0.0
      DO 414 J = 1, N1
         CALL QUADCT(X1(J), Y1(J), X1, Y1, N1, FA, FB, FC, FD)
         CALL QUADCT(X1(J), Y1(J), X2, Y2, N2, GA, GB, GC, GD)
         D1 = MAX(D1, ABS(FA-GA), ABS(FB-GB), ABS(FC-GC),
     *                ABS(FD-GD))
 414  CONTINUE
      D2 = 0.0
      DO 415 J = 1, N2
         CALL QUADCT(X2(J), Y2(J), X1, Y1, N1, FA, FB, FC, FD)
         CALL QUADCT(X2(J), Y2(J), X2, Y2, N2, GA, GB, GC, GD)
         D2 = MAX(D2, ABS(FA-GA), ABS(FB-GB), ABS(FC-GC),
     *                ABS(FD-GD))
 415  CONTINUE
      D = 0.5 * (D1 + D2)
      SQEN = SQRT(FLOAT(N1) * FLOAT(N2) / FLOAT(N1 + N2))
      CALL PEARSN(X1, Y1, N1, R1)
      CALL PEARSN(X2, Y2, N2, R2)
      RR = SQRT(1.0 - 0.5 * (R1**2 + R2**2))
      ZED = D * SQEN / (1.0 + RR * (0.25-0.75/SQEN))
      PROB = PROBKS(ZED)

      RETURN
      END

*******************************************************************

      SUBROUTINE PEARSN(X,Y,N,R)
```

```
      INTEGER N
      REAL    R, X(N), Y(N), TINY
      PARAMETER (TINY=1.E-20)
      INTEGER J
      REAL    AX, AY, DF, SXX, SXY, SYY, T, XT, YT

      AX=0.
      AY=0.
      DO 416 J=1,N
        AX=AX+X(J)
        AY=AY+Y(J)
416   CONTINUE
      AX=AX/N
      AY=AY/N
      SXX=0.
      SYY=0.
      SXY=0.
      DO 417 J=1,N
        XT=X(J)-AX
        YT=Y(J)-AY
        SXX=SXX+XT**2
        SYY=SYY+YT**2
        SXY=SXY+XT*YT
417   CONTINUE
      R=SXY/SQRT(SXX*SYY)
      DF=N-2
      T=R*SQRT(DF/(((1.-R)+TINY)*((1.+R)+TINY)))

      RETURN
      END

*****************************************************************

      FUNCTION PROBKS(ALAM)

      REAL    PROBKS, ALAM, EPS1, EPS2
      PARAMETER (EPS1 = 0.001, EPS2 = 1.E-8)
      INTEGER J
      REAL    A2, FAC, TERM, TERMBF

      A2=-2.*ALAM**2
      FAC=2.
      PROBKS=0.
      TERMBF=0.
      DO 418 J=1,100
        TERM=FAC*EXP(A2*J**2)
        PROBKS=PROBKS+TERM
        IF(ABS(TERM).LE.EPS1*TERMBF.OR.ABS(TERM).LE.EPS2*PROBKS)
     *      RETURN
        FAC=-FAC
        TERMBF=ABS(TERM)
```

```
418    CONTINUE
       PROBKS=1.

       RETURN
       END

******************************************************************

       SUBROUTINE QUADCT(X, Y, XX, YY, NN, FA, FB, FC, FD)

       INTEGER NN
       REAL    FA, FB, FC, FD, X, Y, XX(NN), YY(NN)
       INTEGER K, NA, NB, NC, ND
       REAL    FF

       NA = 0
       NB = 0
       NC = 0
       ND = 0
       DO 419 K = 1, NN
          IF (YY(K) .GT. Y) THEN
             IF (XX(K) .GT. X) THEN
                NA = NA + 1
             ELSE
                NB = NB + 1
             ENDIF
          ELSE
             IF (XX(K) .GT. X) THEN
                ND = ND + 1
             ELSE
                NC = NC + 1
             ENDIF
          ENDIF
419    CONTINUE
       FF = 1. / NN
       FA = FF * NA
       FB = FF * NB
       FC = FF * NC
       FD = FF * ND

       RETURN
       END

******************************************************************
```

## REFERENCES


Adami, C., Nichol, R. C., Mazure, A., Durret, F., Holden, B, & Lobo, C. 1998 *CFHT Information Bulletin* No. 39.

Bahcall, J. 1977 *ARA&A*, **15**, 505.

Bernstein, G. M., Nichol, R. C., Tyson, J. A., Ulmer, M. P., & Wittman, D. 1995 *AJ*, **110**, 1507.

Biviano, A. 1997 *astro-ph*/9711251

Blakeslee, J. P., Tonry, J. L., & Metzger, M. R. 1997 *AJ*, **114**, 482.

Capriotti, F. R. & Hawley, S. L. 1996 *ApJ*, **464**, 765.

Côté, P., Marzke, R. O., & West, M. J. 1998 *astro-ph*/9804319

Cowie, L. L., Henriksen, M., & Mushotzky, R. 1987 *ApJ*, **317**, 593.

Fabian, A. C., Nulsen, P. E. J., & Canizares, C. R. 1984 *Nature*, **310**, 733.

Fasano, G. & Franceschini, A. 1987 *MNRAS*, **225**, 155.

Ferguson, H. C., Tanvir, N. R. & von Hippel, T. 1998 *Nature*, **391**, 461.

Ferrarese, L., *et al.* 1996 *ApJ*, **464**, 568.

Forman, W. & Jones, C. 1982 *ARA&A*, **20**, 547.

Forman, W., Kellogg, E., Gursky, Tananbaum, H., & Giacconi, R. 1972 *ApJ*, **178**, 309.

Freedman, W. L., Mould, J. R., Kennicutt, R. C., & Madore, B. F. 1998 in *IAU Symposium No. 183, "Cosmological Parameters and the Evolution of the Universe", ed. K. Sato* in preparation, (*astro-ph*/9801080).

Gregg, M. D. & West, M. J. 1998 *Nature*, in press.

Gursky, H., Kellogg, E., Murray, S., Leong, C., Tananbaum, H., & Giacconi, R. 1971 *ApJ*, **167**, L81.

Harris, W. E. 1987 *ApJ*, **315**, L29.

Harris, W. E. 1991 *ARA&A*, **29**, 543.

Harris, W. E. 1993 in *ASP Conference Series No. 48, "The Globular Cluster – Galaxy Connection", eds. G. H. Smith & J. P. Brodie*, p. 472.

Harris, W. E. 1996 *AJ*, **112**, 1487.

Harris, W. E., Harris, G. L. H., & McLaughlin, D. E. 1998 *astro-ph*/9801214.

Harris, W. E., Pritchet, C. J., & McClure, R. D. 1995 *ApJ*, **441**, 120.

Harris, W. E. & Pudritz, R. E. 1994 *ApJ*, **429**, 177.

Harris, W. E. & van den Bergh, S. 1981 *AJ*, **86**, 1627.

Hughes, J. P. 1989 *ApJ*, **337**, 21.

Kellogg, E., Tananbaum, H., Giacconi, R. & Pounds, K. 1972 *ApJ*, **174**, L65.

Kendall, M. G. & Stuart, A. 1979 *The Advanced Theory of Statistics* (Griffin, London).

King, I. R. 1966 *AJ*, **71**, 64.

Jones, C. & Forman, W. 1978 *ApJ*, **224**, 1.

Lynds, R. & Petrosian, V. 1986 *BAAS*, **18**, 1014.

Lynds, R. & Petrosian, V. 1989 *ApJ*, **336**, 1.

McLaughlin, D. E., Harris, W. E., & Hanes, D. A. 1994 *ApJ*, **422**, 486.

Merritt, D. 1984 *ApJ*, **276**, 26.

Metcalfe, N., Shanks, T., Fong, R., & JOnes, L. 1991 *MNRAS*, **249**, 498.

Mihalas, D. & Binney, J. 1981. *Galactic Astronomy: Structure and Kinematics, 2ed.* (W. H. Freeman & Company), p. 122.

Oort, J. H. 1977 *ApJ*, **218**, L97.

Peacock, J. A. 1983 *MNRAS*, **202**, 615.

Press, W. H., , Teukolsky, S. A., Vetterling, W. T. & Flannery, B. P. 1992. *Numerical Recipes in Fortran 77: The Art of Scientific Computing, 2ed.* (Cambridge University Press).

Pritchet, C. J. & Harris, W. E. 1990 *ApJ*, **355**, 410.

Salaris, M., Degl'Innocenti, S., & Weiss, A. 1997 *ApJ*, **479**, 665.

Saraniti, D. W., Petrosian, V., & Lynds, R. 1996 *ApJ*, **458**, 57.

Sarazin, C. L. 1988. *X-Ray Emission from Clusters of Galaxies* (Cambridge University Press).

Secker, J., Harris, W. E., Côté, P., & Oke, J. B. 1997 *Proc. "A New Vision of an Old Cluster: Untangling Coma Bernices", Marseille June 1997, Eds. Mazure et al., astro-ph*/9709053.

Soucail, G., Fort, B., Mellier, Y., & Picat, J. P. 1987 *A&A*, **172**, L14.

Sullivan, W. T. III & Johnson, P. E. 1978 *ApJ*, **225**, 751.

Theuns, T. & Warren, S. J. 1997 *MNRAS*, **284L**, 11.

Thompson, L. A. & Valdes, F. 1987 *ApJ*, **315**, L35.

Tremaine, S. P., Ostriker, J. P., & Spitzer, L. 1975 *ApJ*, **196**, 407.

Ulmer, M. P., Wirth, G. D., & Kowalski, M. P. 1992 *ApJ*, **397**, 430.

van den Bergh. 1976 *ApJ*, **206**, 883.

van den Bergh. 1984 *PASP*, **96**, 329.

Vikhlinin, A., Forman, W., & Jones, C. 1994 *ApJ*, **435**, 162.

West, M. J. 1993 *MNRAS*, **265**, 755.

West, M. J., Côté, P., Jones, C., Forman, W., & Marzke, R. O. 1995 *ApJ*, **453**, L77.

White, R. E. III 1987 *MNRAS*, **227**, 185.

---

This manuscript was prepared with the AAS LaTeX macros v4.0.

# Curriculum Vitae

René Kie Tanaja

Born:

Surabaya, Indonesia

January 23, 1973

Permanent Address:

2955 Camrose Dr.

Burnaby, B.C.

Canada

V5A 3W5

Education:

M.Sc., Astronomy,

Saint Mary's University, 1999.

B.Sc., Combined Honours Physics and Astronomy,

University of British Columbia, 1996.

Honours and Awards:

1996 – 97: SMU Graduate Student Scholarship.

1991: UBC University Scholarship.

Relevant Teaching and Working Experience:

1997 – 98: Tutoring, astronomy and physics.

1997, 1998: Occasional substitute teaching, Astronomy class,
Saint Mary's University.

1996 – 98: Astronomy Laboratory Assistant, Saint Mary's University.

1996 – 98: Physics Laboratory Demonstrator, Saint Mary's University.

1996 – 98: Marker, astronomy classes, Saint Mary's University.

1996 – 97: Marker, physics laboratory, Saint Mary's University.

1991: Observations at the Dominion Astrophysical Observatory,
Victoria, B.C.